Global Biogeochemical Cycles

RESEARCH ARTICLE
10.1029/2023GB007875

Atmospheric Methane: Comparison Between Methane's Record in 2006–2022 and During Glacial Terminations

Euan G. Nisbet[1], Martin R. Manning[2], Ed J. Dlugokencky[3], Sylvia Englund Michel[4], Xin Lan[3,5], Thomas Röckmann[6], Hugo A. C. Denier van der Gon[7], Jochen Schmitt[8], Paul I. Palmer[9], Michael N. Dyonisius[10], Youmi Oh[3,5], Rebecca E. Fisher[1], David Lowry[1], James L. France[1,11], James W. C. White[12], Gordon Brailsford[13], and Tony Bromley[13]

[1]Department of Earth Science, Royal Holloway, University of London, Egham, UK, [2]School of Geography, Environment and Earth Sciences, Victoria University of Wellington, Waikanae, New Zealand, [3]NOAA Global Monitoring Laboratory, Boulder, CO, USA, [4]Institute of Arctic and Alpine Research, University of Colorado Boulder, Boulder, CO, USA, [5]Cooperative Institute for Research in Environmental Sciences, University of Colorado Boulder, Boulder, CO, USA, [6]Institute for Marine and Atmospheric Research Utrecht (IMAU), Utrecht University, Utrecht, The Netherlands, [7]Department of Climate, Air and Sustainability, TNO, Utrecht, The Netherlands, [8]Climate and Environmental Physics and Oeschger Centre for Climate Change Research, University of Bern, Bern, Switzerland, [9]School of GeoSciences, University of Edinburgh, Edinburgh, UK, [10]Physics of Ice, Climate and Earth, Niels Bohr Institute, Copenhagen, Denmark, [11]Environmental Defense Fund, London, UK, [12]College of Arts and Sciences, University of North Carolina, Chapel Hill, NC, USA, [13]National Institute of Water & Atmospheric Research Ltd (NIWA), Wellington, New Zealand

Abstract Atmospheric methane's rapid growth from late 2006 is unprecedented in the observational record. Assessment of atmospheric methane data attributes a large fraction of this atmospheric growth to increased natural emissions over the tropics, which appear to be responding to changes in anthropogenic climate forcing. Isotopically lighter measurements of $\delta^{13}C_{CH4}$ are consistent with the recent atmospheric methane growth being mainly driven by an increase in emissions from microbial sources, particularly wetlands. The global methane budget is currently in disequilibrium and new inputs are as yet poorly quantified. Although microbial emissions from agriculture and waste sources have increased between 2006 and 2022 by perhaps 35 Tg/yr, with wide uncertainty, approximately another 35–45 Tg/yr of the recent net growth in methane emissions may have been driven by natural biogenic processes, especially wetland feedbacks to climate change. A model comparison shows that recent changes may be comparable or greater in scale and speed than methane's growth and isotopic shift during past glacial/interglacial termination events. It remains possible that methane's current growth is within the range of Holocene variability, but it is also possible that methane's recent growth and isotopic shift may indicate a large-scale reorganization of the natural climate and biosphere is under way.

Plain Language Summary Atmospheric methane's unprecedented current growth, which in part may be driven by surging wetland emissions, has strong similarities to ice core methane records during glacial-interglacial "termination" events marking global reorganizations of the planetary climate system. Here we compare current and termination-event methane records to test the hypothesis that a termination-scale change may currently be in progress.

Key Points:

- The rapid growth in the atmospheric methane burden that began in late 2006 is very different from methane's past observational record
- Recent studies point to strongly increased emissions from wetlands, especially in the tropics
- This increase is comparable in scale and speed to glacial/interglacial terminations when the global climate system suddenly reorganized

Supporting Information:

Supporting Information may be found in the online version of this article.

Correspondence to:

E. G. Nisbet,
e.nisbet@rhul.ac.uk

Citation:

Nisbet, E. G., Manning, M. R., Dlugokencky, E. J., Michel, S. E., Lan, X., Röckmann, T., et al. (2023). Atmospheric methane: Comparison between methane's record in 2006–2022 and during glacial terminations. *Global Biogeochemical Cycles*, *37*, e2023GB007875. https://doi.org/10.1029/2023GB007875

Received 12 JUN 2023
Accepted 7 JUL 2023

Author Contributions:

Conceptualization: Euan G. Nisbet, Martin R. Manning, Ed J. Dlugokencky, Sylvia Englund Michel, Xin Lan, Thomas Röckmann, Hugo A. C. Denier van der Gon, Jochen Schmitt, Paul I. Palmer, Michael N. Dyonisius, Youmi Oh, Rebecca E. Fisher, David Lowry, James L. France

The air is getting hotter. There's a rumbling in the skies.
I've been wading through the high muddy water, With the heat rising in my eyes.
Bob Dylan: Trying to get to Heaven before they close the door.

1. Introduction

In the past, rapid changes in atmospheric methane have signaled rapid global climate shifts. Does atmospheric methane's recent growth, sustained from the end of 2006 through 2022 and continuing, similarly signal a major global climate shift?

In the modern air, the global methane burden—the total amount of methane in the air—includes both emissions from human activities such as methane from fossil fuel use, agriculture and waste, as well as natural biogenic inputs. Both agricultural and natural emissions are subject to feedbacks from the sensitivity of the biosphere to changes in climate. Summing global biospheric change from measurement data across the planet is a complex

Data curation: Euan G. Nisbet, Martin R. Manning, Ed J. Dlugokencky, Sylvia Englund Michel, Xin Lan, Thomas Röckmann, Hugo A. C. Denier van der Gon, Jochen Schmitt, Paul I. Palmer, Rebecca E. Fisher, David Lowry, James L. France, James W. C. White, Gordon Brailsford, Tony Bromley
Formal analysis: Euan G. Nisbet, Martin R. Manning, Ed J. Dlugokencky, Sylvia Englund Michel, Xin Lan, Thomas Röckmann, Hugo A. C. Denier van der Gon, Jochen Schmitt, Paul I. Palmer, Rebecca E. Fisher, David Lowry, James L. France
Funding acquisition: Euan G. Nisbet, Thomas Röckmann, Paul I. Palmer, James W. C. White, Gordon Brailsford
Investigation: Euan G. Nisbet, Martin R. Manning, Ed J. Dlugokencky, Sylvia Englund Michel, Xin Lan, Thomas Röckmann, Hugo A. C. Denier van der Gon, Jochen Schmitt, Paul I. Palmer, Michael N. Dyonisius, Youmi Oh, Rebecca E. Fisher, David Lowry, James L. France, James W. C. White, Gordon Brailsford, Tony Bromley
Methodology: Euan G. Nisbet, Martin R. Manning, Ed J. Dlugokencky, Sylvia Englund Michel, Xin Lan, Thomas Röckmann, Hugo A. C. Denier van der Gon, Jochen Schmitt, Paul I. Palmer, Michael N. Dyonisius, Youmi Oh, Rebecca E. Fisher, David Lowry, James L. France, James W. C. White, Gordon Brailsford, Tony Bromley
Project Administration: Euan G. Nisbet, David Lowry, James W. C. White, Gordon Brailsford
Resources: Euan G. Nisbet, Paul I. Palmer, James W. C. White, Gordon Brailsford
Supervision: Euan G. Nisbet, Ed J. Dlugokencky, James W. C. White
Visualization: Euan G. Nisbet, Martin R. Manning, Ed J. Dlugokencky, Sylvia Englund Michel, Xin Lan, Thomas Röckmann, Hugo A. C. Denier van der Gon, Paul I. Palmer, Michael N. Dyonisius, Rebecca E. Fisher, David Lowry, James L. France, Gordon Brailsford, Tony Bromley
Writing – original draft: Euan G. Nisbet, Martin R. Manning, Ed J. Dlugokencky, Sylvia Englund Michel, Xin Lan, Thomas Röckmann, Hugo A. C. Denier van der Gon, Paul I. Palmer, Youmi Oh, Rebecca E. Fisher, David Lowry, James L. France, James W. C. White
Writing – review & editing: Euan G. Nisbet, Martin R. Manning, Ed J. Dlugokencky, Sylvia Englund Michel, Xin Lan, Thomas Röckmann, Hugo A. C. Denier van der Gon, Jochen Schmitt, Paul I. Palmer, Michael N. Dyonisius, Youmi Oh, Rebecca E. Fisher, David Lowry, James L. France, James W. C. White, Gordon Brailsford, Tony Bromley

task with large uncertainties, but provided direct anthropogenic forcing can be deducted (a difficult and complex task), the remaining non-anthropogenic growth in biogenic methane emissions provides a direct measure of change.

Unlike CO_2, whose annual cycle is strongly influenced by the spring growth and autumn leaf fall of deciduous plants in the temperate northern hemisphere, the natural methane cycle reflects changes across a much wider latitudinal spectrum, tropical, temperate and Arctic. Natural biogenic sources include tropical and boreal wetlands, ruminants, termites, arctic bogs and permafrost, as well as forest and grassland fires, while anthropogenic biogenic methane comes from agriculture and waste, especially food waste disposal. Aquatic ecosystems, both natural and anthropogenic, contribute up to half the total emissions (Rosentreter et al., 2021).

Starting in 2006 (Figure 1) the atmospheric methane burden has grown strongly (Dlugokencky et al., 2011; Mikaloff-Fletcher & Schaefer, 2019; Nisbet et al., 2014; Schaefer et al., 2016), accompanied by a sustained negative shift in the carbon isotope delta value ($\delta^{13}C_{CH4}$). This shift indicates present-day atmospheric growth is primarily driven by biogenic emissions (Basu et al., 2022; Lan, Basu, et al., 2021; Lan, Nisbet, et al., 2021; Lan et al., 2022; Nisbet et al., 2016, 2019) and not primarily from increased fossil fuel emissions, nor by greatly stronger sink processes. Note that we distinguish between the atmospheric "*burden*"—the total mass of methane in the air expressed in Tg; "*emissions*" or fluxes, in Tg/yr; and *emissions growth* in Tg/yr per year. 1 ppb of methane, as an average mass fraction of the global atmosphere, has a mass of about 2.77 Tg.

Methane's dominant sink is the atmospheric hydroxyl radical [OH], especially in the tropical mid-troposphere, with minor sinks including reaction with atomic chlorine in the marine boundary layer and bacterial methanotrophy in upland and forest soils. The formation and distribution of [OH] is changing as the climatological tropics widen with expansion of the Hadley cells (Nicely et al., 2018). While it remains unclear how much of the observed tropical expansion is within the range of natural variability (Grise et al., 2019), the present rate of increase is exceptional in the long-term record.

The following sections review recent work on the complex and often contradictory puzzle of methane's post-2006 growth. That synthesis is then compared with past events in the glacial paleoclimatological record, where there is strong evidence (Möller et al., 2013) that fast methane rises during rapid glacial to interglacial shifts in the global climate are driven by feedbacks involving tropical wetlands that respond rapidly to warming.

1.1. Feedbacks

Anthropogenic methane emissions have dramatically added to the primary forcing of the climate (Saunois et al., 2020), but the extent of the feedback response of methane emissions as climate has become warmer and wetter remains uncertain (Dean et al., 2018). For methane in particular, it is difficult to separate primary emissions (e.g., gas industry and coal mine leaks) (IEA, 2022), natural feedbacks (e.g., increased wetland emissions) and changing anthropogenic biogenic emissions from farming, sewage, and landfills. As fertilizer production, especially fixed nitrogen, has grown, the productivity of neighboring wetlands may have risen, driven by nitrogen runoff. Rising CO_2 also acts as a fertilizer, globally promoting C3 plant growth (trees and bushes) (Graven et al., 2013; Haverd et al., 2020; Matthews, 2007; Möller et al., 2013), though this impact is eventually limited by supply of nutrients such as fixed nitrogen and phosphorous (S. Wang et al., 2020).

Considering the interlinkages between climate and methane productivity, Dean et al. (2018) concluded that wetlands will form the majority of the methane climate feedback up to the year 2100. Higher primary productivity, in response to warmth, precipitation and inundation, supplies and enhances microbial activity in anaerobic environments. Methanogenic processes may respond more quickly to change than methanotrophic processes (Wen et al., 2018). We may have entered a new era of increased natural methane emissions from wetlands (Rosentreter et al., 2021), driven by multiple feedback factors, including increased rainfall and temperatures, higher rainfall in key areas (Lunt et al., 2021), and higher ecosystem production, aided by agricultural impacts. If present-day feedback responses are indeed strong, then the biogenic component of methane's very strong current growth may be an integrative signal responding to, indicative of, and feeding global-scale change.

Any modern global-scale climate change, by cause and starting point, must be fundamentally different from past changes in the paleoclimate record. Nevertheless, there are strong analogies between methane's current growth and ice core methane records during glacial-interglacial "terminations." In these events, the methane record tracked planetary-scale meteorological reorganizations of the climate system (Broecker & Denton, 1990;

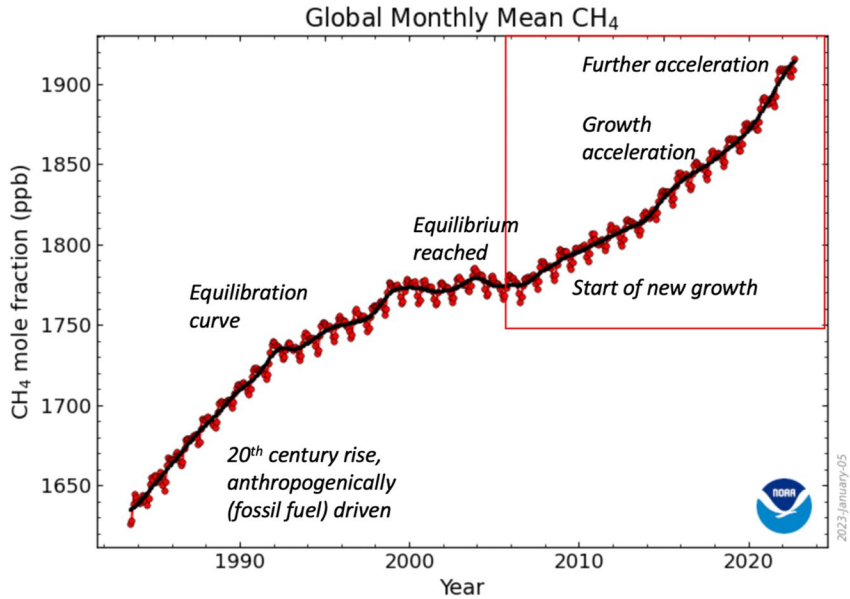

Figure 1. Global monthly mean of atmospheric CH_4, NOAA network. Note convex equilibration curve to 2006; concave acceleration curve from 2007. The convex curve from the 1980s to early 2000s is consistent with relaxation to a source-sink steady state (Dlugokencky et al., 2003), but then the start of a renewed growth became apparent in 2007, and the slope of the new concave curve steepened in 2013 (acceleration of growth), followed by further acceleration in 2020. Modified from Lan et al. (2022). Data from https://gml.noaa.gov/dv/data.html.

H. Cheng et al., 2009; Denton et al., 2010). Thus, the question arises (Nisbet, 2022, 2023): Is methane's modern growth (Figure 2) also a signal that a planetary-scale climate reorganization is underway?

2. Methane Growth, Pre-Industrial Period to Present

There has been strong centennial-scale variation in methane's recent historic record (Figure 3). From Antarctic ice core measurements, Ferretti et al. (2005), Sapart et al. (2012), and Mischler et al. (2009) found that $\delta^{13}C_{CH4}$

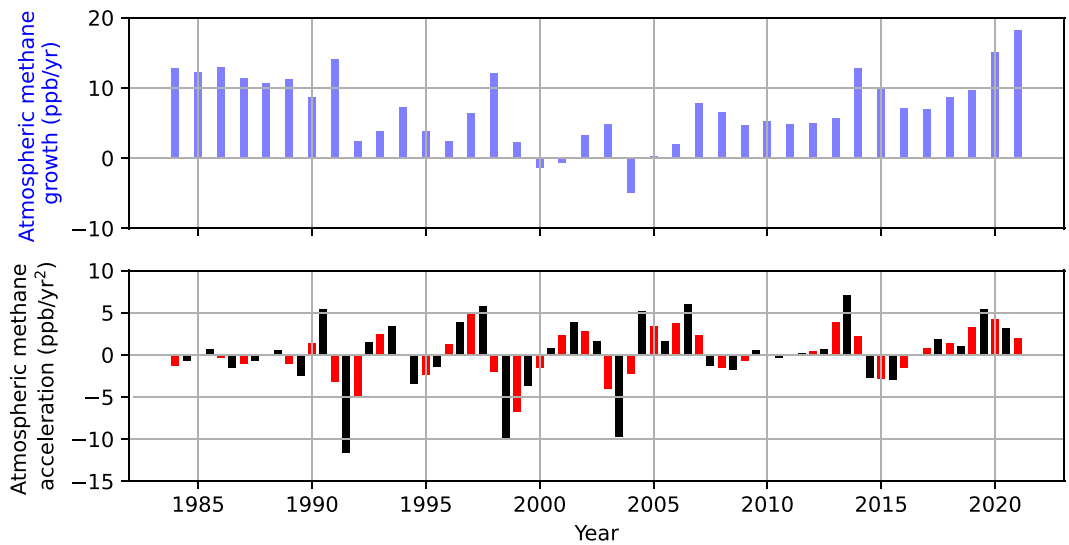

Figure 2. Annual mean growth (blue bars; ppb/yr) and acceleration in half-year intervals (red, black bars; ppb/yr^2) of atmospheric methane inferred from NOAA data, 1984–2022 (NOAA, 2023a). Red bars denote the gradient of the growth rate calculated using second-order accurate central differences of the interior points and first-order accurate one-side differences of the end points. Black bars denote the difference in atmospheric growth between successive years.

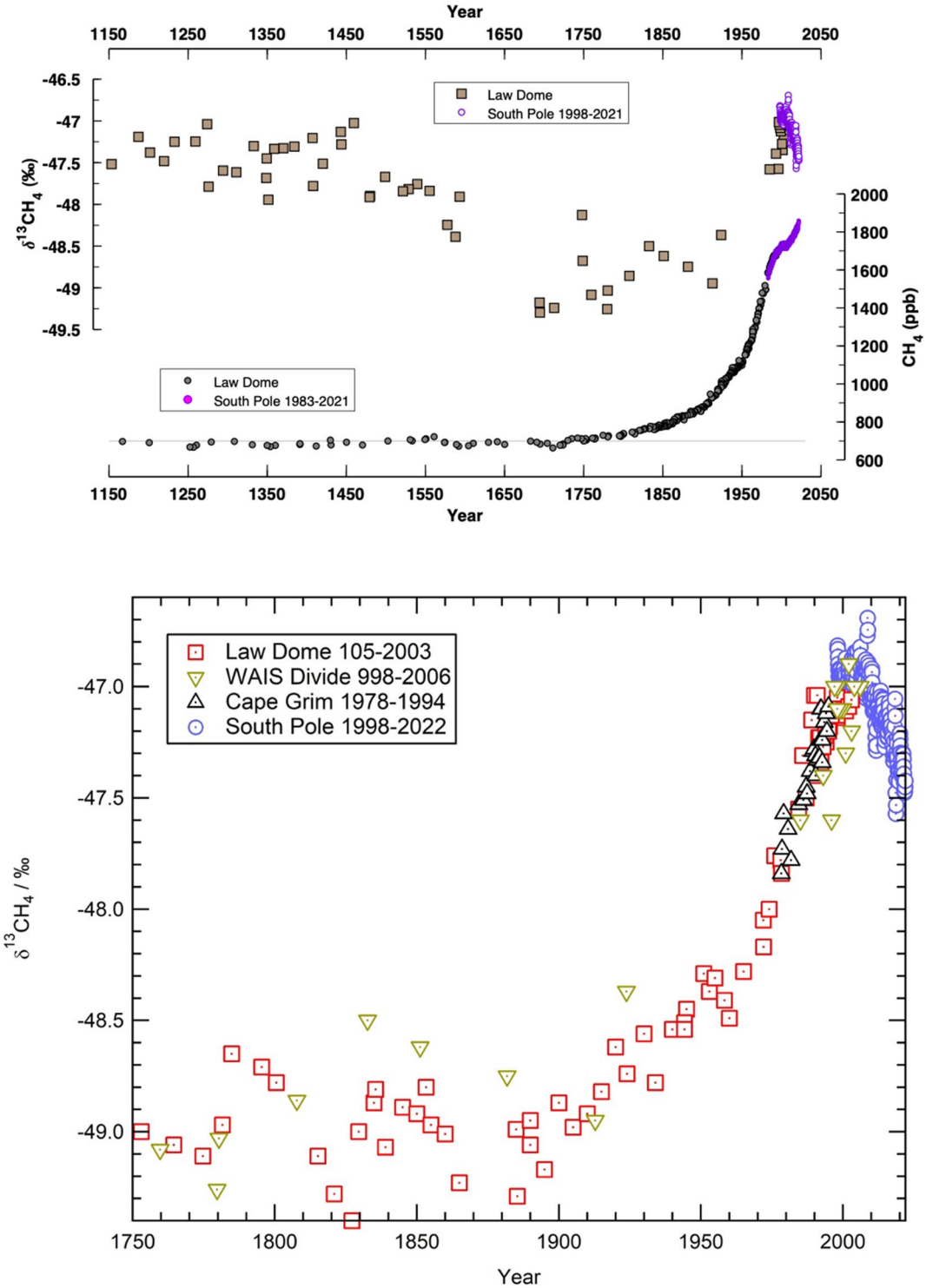

Figure 3. Past records of $\delta^{13}C_{CH4}$. (a) Methane and $\delta^{13}C_{CH4}$ record back to the year 1150 CE, showing the background evolution of both CH4 and $\delta^{13}C_{CH4}$ before the budget was disturbed by human interferences (i.e., before ca. 1500–1600 CE), to indicate historic variability due to changes in climate and wetland emissions on multidecadal or longer time scales. Note the CH_4 background is essentially flat over pre-industrial time, but there is a notable negative trend of about 2‰ between 1500 and 1650 that is gradually reversed as coal-fired industrialization begins. For longer record see Sapart et al. (2012). (b) Post-1750 $\delta^{13}C_{CH4}$ record from South Pole and ice core measurements, showing recent record in more detail. Note long + ve (upwards) trend in $\delta^{13}C_{CH4}$ during the 20th century, driven by fossil fuel emissions, and sustained reversal of trend since 2007. Data from Law Dome: Ferretti et al. (2005); see also Rubino et al. (2019); WAIS Divide: Mischler et al. (2009); Sapart et al. (2012) and from NOAA (https://gml.noaa.gov/aftp/data/trace_gases/ch4c13/flask/surface/).

was about −47‰ around 800 CE, but then showed a strong depletion trend from about 900 CE to 1700 CE, until $\delta^{13}C_{CH4}$ was about −49‰. Prior to the onset of industrialization, in the medieval years from the 12th to the 19th centuries CE, methane rose by around 100 ppb, accompanied by a negative trend in $\delta^{13}C_{CH4}$ from −47.5‰ to −49‰ (Figure 3). Ferretti et al. (2005) interpreted this medieval 2‰ depletion as evidence for a major drop in anthropogenic biomass burning emissions between 800 and 1700 CE, for example, a reduction in deliberate and intense North American grassland burning. CH_4 was rising during this period, implying the reduction in biomass burning emissions must have been more than balanced by other sources. This interpretation is supported by CO evidence from ice cores. Agricultural methane emissions may have helped strengthen the negative trend (Mischler et al., 2009). But that historic depletion rate was about 0.0025‰ per year, totaling less than 0.04‰ over 15 years, very different from what has taken place in the 15 years 2007–2022.

Starting around the years 1750–1800 (Figure 3b), with the onset of coal-fired and then oil and gas-powered industrialization, the $\delta^{13}C_{CH4}$ trend rapidly shifted positive (Etheridge et al., 1998; Ferretti et al., 2005; Lowe et al., 1991; Mischler et al., 2009; Sapart et al., 2012). That exceptionally rapid positive shift accompanying fossil-fuel industrialization from the years 1800–2007 was +2‰ in 250 years, or about 0.01‰ per year, interpreted as evidence that the rise was primarily driven by fossil fuel emissions, first mainly from coal, then with methane emissions as a by-product of oil extraction and use, and more recently from the gas industry too.

In contrast, the ongoing 2007–2022 reverse negative shift in $\delta^{13}C_{CH4}$ has been about −0.55‰ in 15 years: a rate of negative shift four times faster than the positive rise during industrialization, and more than tenfold the rate of the medieval depletion trend. However, it should be noted that many biogenic sources, especially in extra-tropical wetlands, have greater leverage on atmospheric $\delta^{13}C_{CH4}$ than fossil fuel emissions which are closer in source signature to the bulk atmospheric value.

Sustained accurate methane measurement began in the late 1970s and by 1983 NOAA led a co-operative global network collecting flask samples of air from remote sites. Between 1984 and 1990 the growth rate was over 10 ppb/yr, accompanied by a continuing positive shift in $\delta^{13}C_{CH4}$ (Etheridge et al., 1998; Ferretti et al., 2005; Quay et al., 1988), but in the early 1990s Steele et al. (1992) first recognized a slowing-down of growth and predicted stabilization around 2006. This was confirmed by Dlugokencky et al. (1994, 1998, 2003) and Lowe et al. (1994) as the budget equilibrated and the growth rate in fossil fuel emissions slowed. After some years of equilibrium in the early 2000s, the return of growth in the atmospheric methane burden became apparent from late 2006 and into 2007 (Figure 4).

Methane's recent growth is wholly different from the late 20th century pattern. Unlike the convex, equilibrating trend of the late 20th century, growth since the end of 2006 has been on a concave, accelerating trend with the highest growth rates on record in 2020, 2021 and 2022 (Dlugokencky et al., 2011; Lan, Basu, et al., 2021; Lan, Nisbet, et al., 2021; Lan et al., 2022, 2023; Nisbet et al., 2014, 2016, 2019, 2021; Figure 1). Moreover, methane's post-2006 isotopic record is isotopically quite unlike the record of the "fossil-fuel" industrial 19th and 20th centuries. The long trend toward more positive $\delta^{13}C_{CH4}$, indicative of fossil fuel emissions, has unexpectedly reversed, replaced by sustained strong trend to more negative $\delta^{13}C_{CH4}$. The trend is not a subtle statistical drift but rather it is a strong planet-wide shift far outside any plausible statistical variability.

In 2006, the global mean of CH_4 in the marine background air was 1775 ppb, rising to 1912 ppb in 2022, a total rise in the methane burden of 137 ppb (about 379 Tg), or over 150 ppb comparing early 2006 with early 2023. In 2021 alone, growth was near 18 ppb or about 50 Tg. Rapid growth continues with an increase in 2022 of 15 ppb.

Synchronous with the onset of sustained sharp growth in CH_4 has been the isotopic reversal, initiating a sustained strong negative trend in $\delta^{13}C_{CH4}$ (Figures 3 and 4; also Lan, Basu, et al., 2021; Lan, Nisbet, et al., 2021; Nisbet et al., 2019). $\delta^{13}C_{CH4}$ values in Arctic air declined from −47.3‰ in 2006 toward −48‰ in mid-2022. At the South Pole (Figure 4), $\delta^{13}C_{CH4}$ values were about −46.9‰ in 2006, sinking toward −47.4‰ in 2022 (Michel et al., 2022). These trends were constructed from detailed individual flask records (e.g., see Figure S1 in Supporting Information S1 showing the flask-by-flask record from Ascension).

As seen in Figure 4, the last 30 years have had two phases in which CH_4 mole fraction increased, but with these having strong opposite and global trends in $\delta^{13}C_{CH4}$. Longer term records from ice-core and firn air show that this "turnover" in $\delta^{13}C_{CH4}$, has reversed a centuries-long trend toward "heavier" (more ^{13}C-rich) methane that ended around 1998, then a few years of stability, and onset of the current trend toward "lighter" (less ^{13}C-rich) values that began in late 2006 and has been sustained ever since. Globally, the negative $\delta^{13}C_{CH4}$ shift over 2006–2022

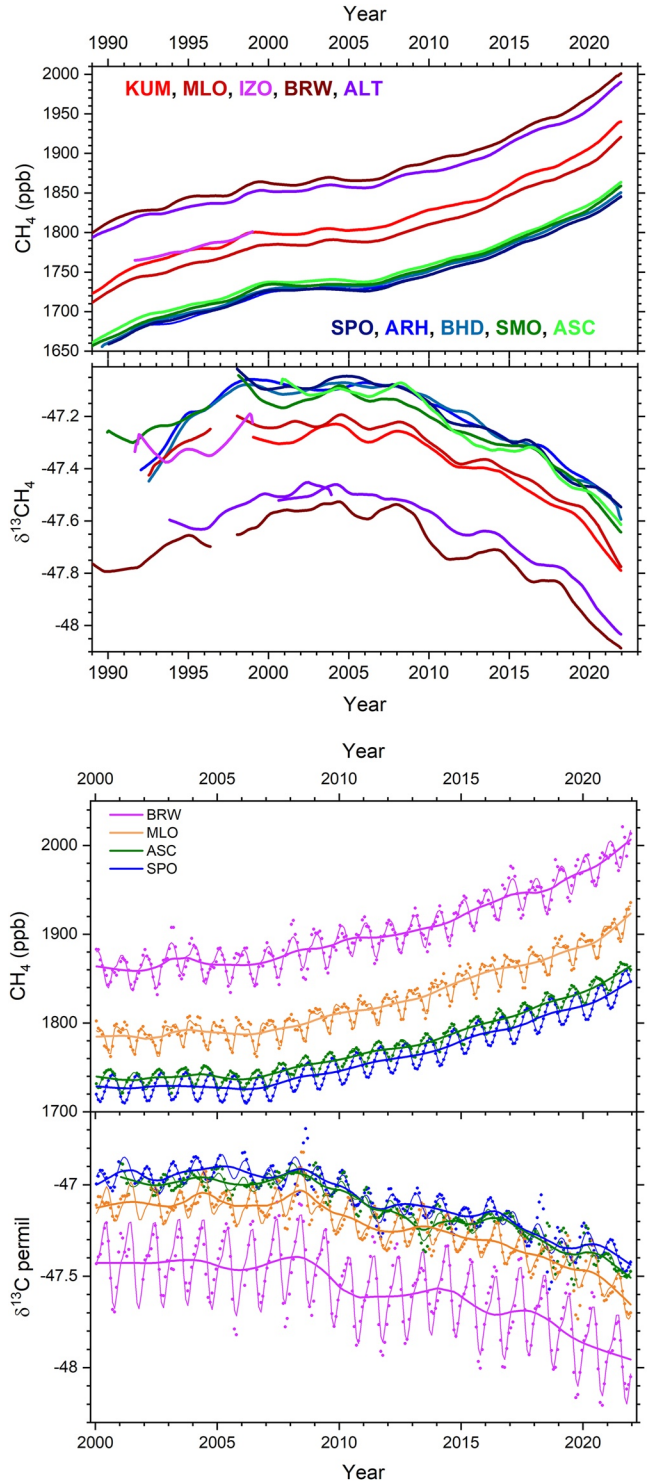

Figure 4.

has been about −0.55‰, from the maximum (most positive) record in March 2008 to the more recent 2022 (Lan, Basu, et al., 2021; Lan, Nisbet, et al., 2021 and update 2023).

Figure 5 shows in detail the "turnover" and seasonality in the remote Southern Hemisphere's $\delta^{13}C_{CH4}$ trend, to illustrate the global evolution. The centuries-long trend toward "heavier" (more ^{13}C-rich) methane ended around

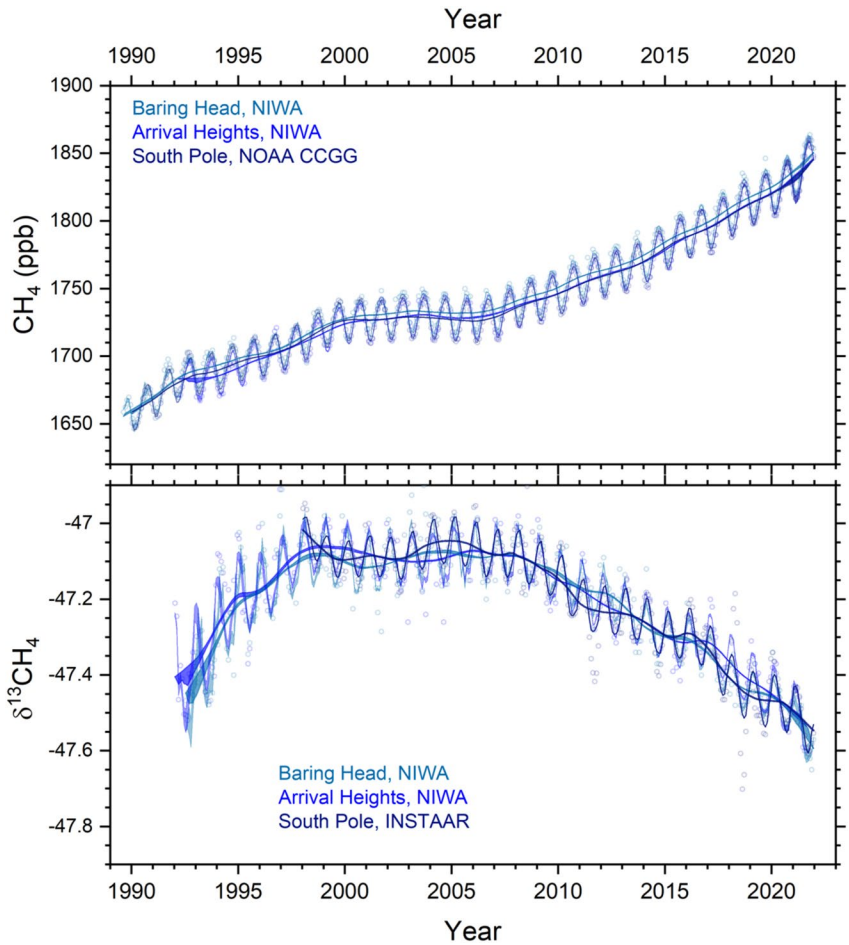

Figure 5. Remote Southern Hemisphere Isotopic Trend since the 1980s. Data from NIWA New Zealand (Baring Head (41°S), Arrival Heights (78°S) and NOAA/INSTAAR measurements (SPO 90°S). See Figure 4 for data sources; intercomparison after Umezawa et al. (2018). https://gml.noaa.gov/aftp/data/trace_gases/ch4c13/flask/surface/). See also Supplementary Note in Supporting Information S1.

1998 (e.g., see Dlugokencky et al., 1994). Then came a few years of stability. The onset of the trend toward "lighter" (less ^{13}C-rich) values began in late 2006 and has been sustained ever since. Globally, the negative $\delta^{13}C_{CH4}$ shift over 2006–2022 has been about −0.55‰, from the maximum (most positive) record in March 2008 to 2022 (Lan, Basu, et al., 2021,Lan, Nisbet, et al., 2021 and update 2023).

3. Methane Sources and Sinks; Isotopic Impacts

The bulk source of global methane emissions has $\delta^{13}C_{CH4} \cong -53‰$ for all sources (Dlugokencky et al., 2011; Nisbet et al., 2019; Sherwood et al., 2017). There is urgent need for better information on isotopic signatures of sources (Thanwerdas et al., 2022). Oh et al. (2022) estimated a mean global wetland $\delta^{13}C_{CH4}$ signature of

Figure 4. Trends in methane mixing ratio (top panels) and $\delta^{13}C_{CH4}$ (lower panels) (a) Trends in methane mixing ratio (top panel) and $\delta^{13}C_{CH4}$ (lower panel) for five long term monitoring sites in each hemisphere. In the Southern Hemisphere the measurement stations are: NOAA's SPO, South Pole (90°S), SMO, Samoa (14°S), and ASC, Ascension (8°S); and NIWA's ARH, Arrival Heights, McMurdo, Antarctica (78°S) and BHD, Baring Head, NZ (41°S). In the Northern Hemisphere they are: NOAA's KUM, Cape Kumukahi (20°N), MLO, Mauna Loa (20°N), BRW, Barrow, Alaska (71°N), ALT, Alert, Canada (83°N), and University of Heidelberg's IZO, Izana (28°N). Early $\delta^{13}C_{CH4}$ data for SMO, MLO and BRW are from Quay et al. (1991) and for IZO from Levin et al. (2012). (b) Detailed patterns showing seasonality for four selected sites, BRW and MLO in the Northern Hemisphere, and ASC and SPO in the Southern Hemisphere. NOAA data. NOAA data from https://gml.noaa.gov/aftp/data/trace_gases/ch4c13/flask/surface/. NIWA data in the World Data Center for Greenhouse Gases https://gaw.kishou.go.jp/. For further details of specific records see Supporting Information S1. Intercomparison follows Umezawa et al. (2018). SPO and MLO are at 2,810 and 3,397 m elevation respectively but the other points are close to sea level. Details of the data from these sites are shown in Supporting Information S1 while this figure summarizes the similar patterns seen globally. See also Supplementary Note in Supporting Information S1.

−61.3 ± 0.7‰. This reflects a mix between northern high-latitude C3 plant wetlands (mean −67.8‰) and tropical C4-rich wetlands (mean −56.7‰) (Dlugokencky et al., 2011; Ganesan et al., 2018; MOYA/ZWAMPS Team et al., 2021; Quay et al., 1988; Menoud et al., 2022; Sherwood et al., 2017). Note the means and precisions cited here are from partial and perhaps unrepresentative sampling: real world averages may be several ‰ different. In addition to the global C3/C4 plant distribution, the distribution of hydrogenotrophic/acetoclastic methanogens and vegetation-specific CH_4 transport all contribute to the $\delta^{13}C_{CH4}$ variability of wetland emissions (Ganesan et al., 2018). France et al. (2021) found methane from South American and African southern outer tropical (seasonal) wetlands had $\delta^{13}C_{CH4}$ −60 ± 5‰ while equatorial wetlands emitted methane with $\delta^{13}C_{CH4}$ −52 ± 2‰. Similarly, Oh et al. (2022) found tropical wetland emissions are enriched by about 11‰ relative to boreal wetlands.

Agricultural emissions, like wetland emissions, vary with latitude and C3/C4 proportions in ruminant diets (Menoud et al., 2022), and tropical measurements are scarce. For rice fields, France et al. (2021) found $\delta^{13}C_{CH4}$ −61 ± 4‰. Farmed ruminant emissions vary with diet, with a global average $\delta^{13}C_{CH4}$ perhaps around −65‰ (e.g., J. Chang et al., 2019), but data are scarce from tropical ruminants where C4 fodder can dominate; for example, for Kenyan pastured cattle, $\delta^{13}C_{CH4}$ is around −57‰ (MOYA/ZWAMPS Team et al., 2021). Fossil fuel emissions have $\delta^{13}C_{CH4}$ globally roughly between −43‰ and −45‰ (Lan, Basu, et al., 2021). However, $\delta^{13}C_{CH4}$ values range widely from highly positive values (e.g., −25‰ for some gasfields) to very negative (as light as −70‰ in some cases). Howarth (2019) suggested that about a third of growth in methane emissions from all sources globally over the past decade came from shale gas production in North America. Nevertheless, Milkov et al. (2020), Basu et al. (2022), and Z. Zhang et al. (2023) showed this to be unlikely.

The steady-state lifetime for atmospheric methane is between 9 and 10 years (Dlugokencky et al., 2011; Ehhalt, 1974; Lan, Basu, et al., 2021; Nisbet et al., 2019). Methane's perturbation lifetime, which accounts for atmospheric chemistry relaxation times and is more relevant for climate impacts of emission reductions, is approximately 12 years (Myhre et al., 2013; Prather et al., 2012). Methane's main sinks, atmospheric hydroxyl [OH], Cl, and soil methanotrophy, are all subject to interannual variability as well as to the growth in the methane burden. Nicely et al. (2018) found the expected decline in [OH] caused by methane growth was largely offset by positive trends in tropospheric [OH] responding to changes in water vapor, NO_x, and O_3. Methane's sinks all respond to climate change. Yin et al. (2021) showed that the longer-term impact of [OH] changes was modest, a conclusion updated by Basu et al. (2022). Similarly, Thompson et al. (2018) and Drinkwater et al. (2022) also found the impact of changes in the atmospheric sink did not appear to be a key driver of methane's strong and sustained growth. However, in some years specific events can have large impacts on methane growth. In particular, [OH] fluctuations can make a major contribution to methane growth in hot El Niño years (Zhao et al., 2020), especially when there are enhanced CO emissions from biomass burning, as CO competes with CH_4 for [OH]. Such effects smooth out during a full El Niño/Southern Oscillation (ENSO) cycle, as CO emissions from biomass burning decrease again in subsequent cool, regionally wet La Niña years.

Sources and sinks show interannual variability and may have been affected by COVID lock-downs in 2020 (Laughner et al., 2021), though that transient impact is unlikely to have been sustained significantly into 2021 and 2022. For the unusual year 2020, when anthropogenic emissions of air pollution were much affected by COVID lockdowns (e.g., Cooper et al., 2022), the growth in methane was driven both by a decline in [OH], and by increased wetland emissions (Peng et al., 2022), especially in the tropical and sub-tropical Northern Hemisphere and in western Siberia and central Canada. Using analysis of GOSAT retrievals, Qu et al. (2022) concluded 14% of growth was from [OH] changes. Likewise, Feng et al. (2023) also found an [OH] reduction comparable to Peng et al.'s results, but concluded that most of the observed increase in atmospheric methane during 2020 and 2021 was caused by increased emissions, especially in Eastern Africa. The full causes of methane's remarkable growth in 2021 and 2022, when COVID lockdowns were less severe, are still being debated but it is notable that over the period 2020–2022 the methane growth histogram matches the very unusual “triple-dip” 3-year La Niña event (NOAA, 2023b).

Methane's minor sinks are destruction by atmospheric chlorine (Hossaini et al., 2016), oxidation by soil methanotrophs, and upward transport into the stratosphere where methane is destroyed (and isotopically fractionated) by photooxidation. Methane destruction by chlorine is particularly interesting: although it only accounts for ∼2.5% of the total methane sink (but with larger regional-scale effects, Hossiani et al., 2016), it is highly fractionating for C and H isotopes (Strode et al., 2020). Moreover, it is possible that Cl production when mineral dust mixes with

sea spray aerosol has been underestimated. If so, total global biogenic methane emission may have been underestimated by around 2% (van Herpen et al., 2023). All these sinks will have interannual variability, especially in the ENSO cycle, and will also be subject to changing feedbacks to long-term climate warming.

All biological methane sources, both purely "natural" and anthropogenic, respond to climate change and the rapid strong positive feedbacks make methane an excellent integrating indicator of large-scale wetland ecosystem change. Increased warmth and moisture in the "wet tropics" are likely to increase plant growth and thus ruminant productivity, and also microbial activity in manure and wetlands. In the boreal and Arctic realms warmth is also likely to increase wetland emissions. Moreover, as mentioned above (Section 1.1), CO_2 acts as a potent fertilizer for C3 plants, increasing plant productivity (Haverd et al., 2020; Lobell & Field, 2008; Uddin et al., 2018) and thus supply of organic matter to eventual anaerobic decay, though it is possible this impact is eventually limited by supply of nutrients, primarily fixed nitrogen and phosphorus (S. Wang et al., 2020).

4. The Wetland Hypothesis

The wetland hypothesis is that biogenic emissions, particularly from wetlands, are growing rapidly and are the dominant cause of recent growth (Basu et al., 2022; Lan, Basu, et al., 2021; Lan, Nisbet, et al., 2021; Lunt et al., 2019; Oh et al., 2022, Z. Zhang et al., 2023). Aquatic ecosystems are enormously important in the global methane budget (Rosentreter et al., 2021). Dean et al. (2018) found wetland emission growth can be primarily ascribed to climate change feedbacks. Table 1 provides a highly simplified comparison of results from recent studies in a very active and complex field.

The "wetland hypothesis" has been supported by powerful evidence that increased wetland emissions, especially in the tropics, drove methane's exceptional growth in 2020 (Feng et al., 2022, 2023; Lunt et al., 2019, 2021; Peng et al., 2022; Qu et al., 2022). The isotopic evidence is strong. Using a process-based biogeochemistry model, Oh et al. (2022) concluded the spatial distribution of wetland $\delta^{13}C_{CH4}$ emissions is consistent with the observed latitudinal gradient in $\delta^{13}C_{CH4}$, implying the growth in microbial emissions has been the dominant driver for methane's post-2006 rise and concurrent negative trend in $\delta^{13}C_{CH4}$. The causes of increased wetland emissions likely include increased rainfall and inundation in drainage basins (Feng et al., 2022; Lunt et al., 2019, 2021; Pandey et al., 2017), and also overall warm temperatures in the post-2006 period, as plant and microbial productivities rise with temperature, provided water and nutrients are available.

Methane's remarkable growth in 2020–2022 has been synchronous with an unusual La Niña event (Hasan et al., 2022) with a "triple-dip" 3-year period (McPhaden et al., 2023) that has brought sustained seasons of exceptional rainfall to many important regions in the moist tropics. However, emissions from aquatic systems are highly variable (Rosentreter et al., 2021), and inherently difficult to parameterize (Ringeval et al., 2014).

Because cloud cover is typically deep and persistent during wet seasons over key emitting regions, it is difficult to study tropical wetland emissions in rainy season using satellite remote sensing directly overhead, but the long atmospheric lifetime of methane allows for these emissions to be quantified via observations collected downwind. Feng et al. (2022) used satellite observations to infer that over 80% of the observed growth in the global methane burden between 2010 and 2019 came from tropical emissions. Separately, Feng et al. (2023) estimated that 66% of methane's global increase in 2020 was due to increased emissions, particularly from the tropics. They found evidence for growing microbial sources over the tropics with a very large increase (14 ± 3 Tg) in recent (2020) emissions from northern hemisphere Eastern Africa (e.g., the Nile Sudd—see Lunt et al., 2019), while emissions decreased in China and India.

These results are supported by the findings of Qu et al. (2022) from GOSAT retrievals, that 82% of methane growth from 2019 to 2020 was primarily driven by increased emissions rather than [OH] sink reductions, with a large contribution from African wetlands. Similarly, Drinkwater et al. (2022) found methane recent growth (2004–2020) has been driven by a progressive increase in emissions, with emissions from tropical and sub-tropical sources (30°N to 30°S, i.e., including the monsoonal climate belt) accelerating by 3.8 Tg/yr/yr. They concluded methane's growth was primarily driven by biogenic emissions, especially from regions with large wetlands, with increases in annual emissions over the period of about 17 Tg from Northern Hemisphere Africa, and 21 Tg from Tropical South America, though Chinese annual emissions also increased very strongly (27 Tg).

Anthropogenic impacts can also increase wetland emissions. Although widespread drainage of wetlands is also taking place, tropical wetlands in Africa can host large cattle populations (own observations). Indirect

Global Biogeochemical Cycles
10.1029/2023GB007875

Table 1
Simplified Comparison: Examples of Some Recent Assessments of Wetland Emissions and Their Growth

(a) Examples of some estimated outer tropical wetland emissions

Location	Latitude, area	Emissions Tg/yr	Reference
Bangweulu, Upper Congo basin, Zambia	11°S, >10,000 km^2	1–3	Shaw et al. (2022)
Pantanal, Brazil	Around 17°S, around 150,000 km^2	2–3.3	Gloor et al. (2021)
Llanos de Moxos, Bolivia	Around 12°S–15°S, Around 70,000 km^2	3.6	France et al. (2022)
Freshwater wetlands	*Global*	138–165	Rosentreter et al. (2021)
East Africa	*Regional*	March–May 2018: 6 Tg	Lunt et al. (2021)
		October–December 2019: 9 Tg	
South Sudan	*Regional*	7.4 ± 3.2 Tg	Pandey et al. (2019)

(b) Global emissions growth (all sources) in the single years 2020 and 2021

Period	Emissions growth in year (Tg)	Reference
2020	27	Feng et al. (2023)
2021	21	Feng et al. (2023)
2020	25–37 (48% from Africa)	Qu et al. (2022)

(c) Global wetland-only emissions growth in the single years 2020 and 2021

Period	Emissions growth in year (Tg)	Reference
2020	14–26	Z. Zhang et al. (2023)
2021	13–23	Z. Zhang et al. (2023)
2020	6–7	Peng et al. (2022)
2019–2020	22–32 (of which 15 in Africa)	Qu et al. (2022)

(d) Global emissions in the years from the onset of growth prior to 2020

Reference	Period	Growth in biogenic emissions Tg/yr	Estimated emissions growth acceleration Tg/yr/yr
Basu et al. (2022)	2007–2012	26	4
Basu et al. (2022)	2013–2017	32	
Z. Zhang et al., 2023	2007–2021	8–10	1.3–1.4
Oh et al., 2022	2006–2016	28 assumed scenario	

Note. Numbers given here are for comparison purposes only. See cited sources for original details and data. Numbers here highly simplified, rounded off from the disparate results in the many cited studies, and are very approximate with large uncertainties. Italics refer to areas including multiple wetlands.

anthropogenic forcing factors include CO_2 fertilization (Haverd et al., 2020; Holden et al., 2013), run-off to wetlands from nitrogen fertilizer application (Ackerman et al., 2019), sulfate deposition (Gauci et al., 2005) in regions like southern Africa and China with large coal-industry emissions, and perhaps also the complex impacts of human predation on wetland fauna. The fertilizing impact of run-off from arable croplands into nearby wetlands by nitrogen fertilizers (Fowler et al., 2013) may be important. However, most boreal wetlands are far from farming drainage, while in many parts of the tropics, although fertilizer application in arable lands around wetlands is increasing rapidly (e.g., Uganda), the use of fertilizers is still very low compared to farming in northern temperate regions (Dangal et al., 2019; FAO, 2017; IFAstat, 2022; Ludemann et al., 2022).

In particular, CO_2 fertilization of C3 plants may be important. There is evidence (Möller et al., 2013) for CO_2 fertilization impact in past transitions: the strong correlation between $\delta^{13}C_{CH4}$ and CO_2 in the ice core record of the past 160 ka is much better than the correlation between $\delta^{13}C_{CH4}$ and CH_4. This suggests CO_2 fertilization was an active feedback in past changes by increasing plant productivity and hence microbial methane emissions during the initiation of interglacial episodes, with isotopic impacts favoring C3 plants (more negative $\delta^{13}C_{CH4}$) over C4 grasses. Thus the glacial/interglacial $\delta^{13}C_{CH4}$ record may reflect in situ shifts in plant populations and productivity as well as shifts in the geographic loci of emission. However, on the modern planet this impact is difficult to assess. It is also likely that nitrogen cycle constraints and phosphorus availability may be progressively limiting the effect of CO_2 fertilization (Huntingford et al., 2022; S. Wang et al., 2020).

Wetland models have large uncertainties (K. Y. Chang et al., 2023) and tropical wetland emissions may be much larger than hitherto inferred in land surface models of wetland methane sources (Nisbet, 2023; Shaw et al., 2022; Z. Zhang et al., 2023). Recent tropical wetland field campaigns that included both low-flying aircraft and on-ground sampling have shown that emissions from some wetlands are very substantial indeed (Table 1). For example, overflying the Llanos de Moxos wetlands in Bolivian Amazonia in March 2019 (late wet season), France et al. (2022) found extremely large methane enhancements (500 ppb over background). These were inferred to have come from very high surface fluxes of methane. Annual emissions were estimated around 3.6 Tg/yr from the Llanos de Moxos wetlands. Further south, in the Pantanal wetlands of Brazil and Bolivia in the South American seasonal outer tropics, Gloor et al. (2021) used a planetary boundary layer budgeting technique to estimate the Pantanal's total regional emissions of 2.0–2.8 Tg/yr, while their Bayesian inversion using an atmospheric transport model found even higher emissions of ∼3.3 Tg/yr.

At about the same southern outer tropical (seasonal) latitude in Africa, from an aircraft campaign in February 2019 (mid-wet season) in the Upper Congo Bangweulu wetlands of Zambia, Shaw et al. (2022) derived very large emissions of 1.2–3.0 Tg/yr. Bangweulu is only part of the Upper Congo's extensive suite of wetlands. Emissions from Zambezi basin wetlands were also significant (Shaw et al., 2022). This work suggests total emissions from wetlands in the Congo and Zambezi basins may be very large. Interestingly, the regional $\delta^{13}C_{CH4}$ isotopic signatures of emissions of outer (single rainy season) tropical C4/C3 wetlands in Zambia and Bolivian Amazonia were very similar, around −59‰ to −60‰ (France et al., 2021; MOYA Team et al., 2021), presumably reflecting the similarity of the seasonal outer tropical C4/C3 vegetation mix.

Unfortunately, on-ground or low-level aircraft/UAV in situ monitoring of major tropical wetlands is inadequate (Nisbet, 2023; Ringeval et al., 2014), so it is not possible to use *in-situ* monitoring to confirm year-on-year changes. From satellite observations, Lunt et al. (2021) found strong XCH_4 enhancements in East Africa consistent with large positive seasonal precipitation anomalies. Zonal observations from remote stations of the NOAA network (Nisbet et al., 2016, 2019) broadly support the findings of increased wetland emissions. Interannual rainfall and temperature variability can be very large (Lunt et al., 2021; Palmer et al., 2023; Peng et al., 2022), depending on shifts in the position and intensity of the Inter-Tropical Convergence Zone (ITCZ). Thus expansion and intensification of the tropical Hadley cell circulation can have dramatic impacts on methane emissions.

To turn to bottom-up assessments, Z. Zhang et al. (2023), applying climate data from meteorological stations and reanalysis in a land surface wetland model, found that climate change impacts increased annual wetland emissions by 8–10 Tg/yr in 2007–2021 compared to the 2000–2006 level. Specifically, they also found huge positive anomalies of 14–26 Tg in 2020 and 13–23 Tg in 2021, and that tropical methane emissions contributed a large part of methane's growth in those 2 years. For the single year 2020, compared to 2019, the bottom-up estimate of Peng et al. (2022) found an increase in wetland emissions of 6.0 ± 2.3 Tg. Their top-down 3D atmospheric inversion gave a global increase in surface emissions of 6.9 ± 2.1 Tg/yr between 2019 and 2020, which they also mostly attributed to increased wetland emissions. These very large increments are consistent with the

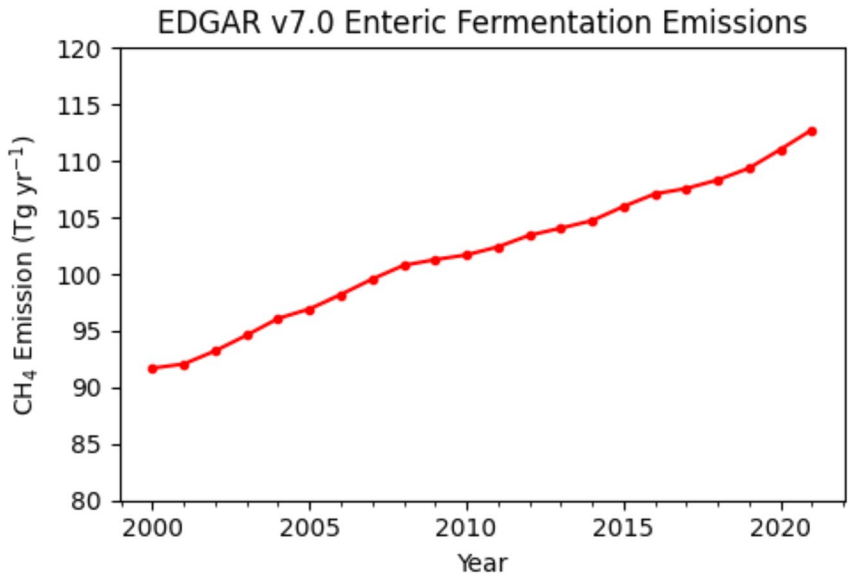

Figure 6. Estimated growth in methane emissions from enteric fermentation (ruminants), from EDGAR (2023). See Table 2. Recent (2010–2021) growth rate about 1 Tg/yr/yr.

hypothesis that growth has been supercharged by precipitation in the unusual 2020–2022 La Niña "triple dip" event (McPhaden et al., 2023; NOAA, 2023b), though it should be noted that earlier intense La Niña events did not coincide with years of especially extreme methane growth.

5. Agricultural, Biomass Burning, and Waste Emissions

Agriculture is a major source of biogenic methane emissions, from cattle breath ($\delta^{13}C_{CH4}$ slightly more negative than the bulk methane burden), wetland rice cultivation, and biomass burning ($\delta^{13}C_{CH4}$ much more positive than the burden) (for isotopic signatures of sources see Dlugokencky et al., 2011; MOYA/ZWAMPS Team et al., 2021; Nisbet et al., 2016, 2019).

Livestock emissions are growing but the rate of growth is difficult to quantify. L. Zhang et al. (2022) estimated, with uncertainty around 20%, that methane emissions from global livestock populations were around 105 Tg in 2000, 121 Tg in 2011, and 132 Tg in 2019, growing by 27 Tg from 2000 to 2019, or 1.4 Tg/yr/yr. Using an inversion framework to verify methane emissions from satellite-based observations, J. Worden et al. (2023) reported a growth rate of livestock emissions of 0.25–1.3 Tg/yr/yr. The growth rate they estimated was similar to EDGAR results, although J. Worden et al. (2023) considered the EDGAR assessment had underestimated livestock emissions. From 2000 to 2020, the EDGAR (2023) assessment finds an increase in emissions from enteric fermentation of 20–21 Tg (Figure 6), with another 2 Tg increase from animal manure (EDGAR, 2023) but no significant acceleration in the rate of increase in the past decade. Our assessment (Figure 6) of growth in ruminant emissions from enteric fermentation, estimated from the EDGAR (2023) database, is nearly 1 Tg/yr/yr for 2000–2020 (Table 2), somewhat less than the L. Zhang et al. (2022) estimate but within the very wide uncertainties.

The densest cattle populations are in South Asia, tropical Africa and tropical South America. Livestock population growth will be facilitated by increased grazing and browsing productivity in a warmer wetter climate. However, it is not clear how much agricultural expansion in the tropics has increased total land surface methane emission. Africa and more recently South America are undergoing a widespread transition from a complex "natural" ecology of diverse ruminants and pseudo-ruminants to a now human-dominated pastoral system of cattle, goats and sheep (e.g., see L. Zhang et al., 2022).

In the "natural" African ecology, ruminants from browsing giraffe to grazing buffalo exploit all parts of the floral variety. In contrast, in cattle-dominated monocultures, where most or all natural ruminants are eliminated, food production specifically for the very rapidly growing human populations will have increased, but the total body mass per unit area of the ruminants that are producing methane may not be larger (e.g., see data in Taylor and

Table 2
Anthropogenic Methane Emissions in the Years 2000, 2010, and 2020 and Decadal Growth Rate in the Last Two Decades

IPCC sector	Emission Tg yr^{-1} CH_4			Growth rate (Tg CH_4 yr^{-2})	
Year	2000	2010	2020	2000_2010	2010_2020
1 Energy	103.51	123.98	137.42	2.05	1.34
2 Industrial processes and product use	0.19	0.33	0.49	0.01	0.02
3 Agriculture, forestry and other land use	137.41	151.93	162.47	1.45	1.05
3A1 Enteric Fermentation	91.70	101.69	111.03	1.00	0.93
3A2 Manure Management	10.87	11.69	12.54	0.08	0.08
3C1 Biomass Burning	1.35	1.71	1.96	0.04	0.03
3C7 Rice Cultivations	33.49	36.84	36.94	0.33	0.01
4 Waste	62.72	70.60	83.58	0.79	1.30
4A Solid Waste Disposal	29.64	30.65	35.65	0.10	0.50
4B Biological Treatment of Solid Waste	0.17	0.23	0.28	0.01	0.01
4C Incineration and Open Burning of Waste	1.14	1.32	1.55	0.02	0.02
4D Wastewater Treatment and Discharge	31.76	38.40	46.10	0.66	0.77
5 Other	0.15	0.15	0.15	0.00	0.00
Total anthropogenic	303.98	346.99	384.11	4.30	3.71
Total "microbial anthropogenic" (excluding FF etc.)[a]	197.98	219.98	243.18	**2.2**	**2.3**

Note. Data from EDGARv7.0 (Crippa et al., 2021; EDGAR, 2023). "Bottom up" estimates with wide uncertainties.
[a]excludes Energy (1), Biomass burning (3C1), and Incineration and open burning of waste (4C). Values in Bold (microbial anthropogenic) discussed in text.

Walker (1978)). Moreover, much tropical cattle manure falls on dry pastures in aerobic conditions not supportive of methanogens, although it should be noted that in some parts of Africa cattle are kept overnight in "bomas" (corrals) where manure collects under urine and methane emissions can be significant (Leitner et al., 2023). Thus the overall net change in methane emissions from replacing an original productive and diverse natural ecology with anthropogenic cattle or maize monocultures is unclear.

Biomass burning emissions come from incomplete combustion. The amount of burning varies from year to year, which has significant impact on emissions (J. R. Worden et al., 2017). In the tropics, biomass fires are closely linked to changes in the ITCZ and the ENSO cycle. Grassland fires (mainly C4 plants in the tropics) are widespread in dry winters after good rainy seasons, often covering very large areas. Crop waste fires also occur mainly in dry season, varying with precipitation in the previous wet season. These fires, particularly of ^{13}C-rich tropical C4 crop plants like maize, sugarcane, and millet, emit isotopically heavy methane.

Burning of tropical C3 woodland and forest also occurs, especially in clearing land. Tracking biomass burning is difficult: satellite observation quantifies burnt area but it is more difficult to assess fuel load and intensity of fire (especially important in crop waste fires). Barker et al. (2020) found high variability in emissions measured in flights over active fires, with methane emissions of 1.8 ± 0.19 g/kg of fuel over outer-tropical Senegal, but 3.1 ± 0.35 g/kg over equatorial Uganda. Boreal biomass burning, in contrast, is mainly wildfire in northern C3 forests, highly dependent on summer temperatures, and more easily assessed by remote sensing.

"Biogenic" CO is mainly produced by biomass burning, but the CO record in the 2000–2010 decade is affected by Europe's decade of "dieselization" favoring diesel-fuel passenger cars, which are low emitters of CO compared to petrol engined cars. Contrasting the period 2001–2007 to the 2008–2014, J. R. Worden et al. (2017) concluded biomass burning emissions of methane decreased by 3.7 (±1.4) Tg CH_4 per year, and this drop may have contributed to the standstill in methane growth in the early years of the 21st century. For the periods 2007–2012 and 2013–2017, inversions of both mixing ratio and isotopic data suggest overall global pyrogenic emissions dropped slightly or showed little change (Z. Zhang et al., 2021, comparison in Basu et al., 2022).

Much agricultural growth comes from expansion of farmed land area, displacing natural ruminants from grasslands or cutting forest and draining wetlands and burning peatlands. Thus, for tropical agricultural emissions it

is difficult to allocate proportions of "feedback-driven" and "technology-driven" emissions growth. The impact on crop yields and ruminant fodder supply of indirect factors such as CO_2 fertilization and sulfate deposition, is not easily quantified.

Bottom-up (EDGAR, 2023) inventories suggest anthropogenic emissions from wastewater, solid waste, and landfills are increasing worldwide. Despite successful efforts to reduce waste emissions in Europe and other regions, the rapid growth of tropical cities is driving increased urban waste disposal and these emissions are very poorly quantified (Nisbet et al., 2020). Waste disposal in tropical cities is increasing in large poorly managed landfills (Nisbet et al., 2020), but food waste comes from local agriculture, so waste emissions are linked to local agricultural productivity. In the EDGAR v7.0 inventory (EDGAR, 2023) the estimated growth of annual solid waste and landfill emissions from 2006 to 2021 is about 5.7 Tg, while methane from wastewater has increased by about 11 Tg/yr over the same period.

The "climate feedback" proportion of growth in emissions of methane from tropical agricultural and waste disposal is uncertain. Growth in ruminant and landfill biogenic emissions depends both on global change feedbacks (more productivity in a warmer, wetter, CO_2-rich environment) and also on "direct-action" factors increasing agricultural productivity such as nitrogen fertilizer application and genetic modification of seeds.

Overall, including solid and liquid waste, manure handling and enteric fermentation in agricultural ruminants, EDGAR inventory data (Table 2) suggest microbial methane emissions from anthropogenic activities rose each year by about 2.3 Tg/yr, or an increase of about 35 Tg from the end of 2006–2020. Although there is wide uncertainty on these bottom-up estimates, they appear broadly consistent with top-down estimates. Importantly, there is no evidence in the data for a sudden acceleration in the growth of agricultural and waste emissions post-2006.

6. Inference: Increased Natural Emissions Are a Major Cause of Recent Methane Growth

Quantifying emissions from "natural" sources as they respond to climate change is difficult. Ongoing experimental measurement of methane fluxes from wetlands is minimal, especially in Africa. An alternative is to use isotopic information to assess global total (i.e., natural and anthropogenic) biogenic emissions and then subtract bottom-up estimates of emissions from biogenic sources under anthropogenic control, with the caveat that these too respond to climate warming.

Studying the period 1999–2016, Basu et al. (2022) estimated methane's 2008–2014 rise was driven by global emissions growth of 27.1 ± 0.6 Tg yr^{-1} or, nearly 4 Tg/yr/yr. They found the negative shift in $\delta^{13}C_{CH4}$ can be balanced by assuming about 15%, or 50 Tg, of the total recent rise is from growth in fossil fuel emissions (i.e., with $\delta^{13}C_{CH4}$ more positive than the methane already in the air). Comparing the period 2007–2012 with the period 2013–2017, Basu et al. (2022) found an increase in biogenic emissions of 32.3 ± 3.2 Tg/yr. After 2017 and especially in 2020–2023, the burden grew more rapidly.

Similarly, looking at the surge in growth in 2019–2020, using a global inverse analysis of GOSAT satellite observations, Qu et al. (2022) found the imbalance between sources and sinks of methane increased by 31 Tg in the year 2019–2020. They found that half the growth in methane emissions in 2019–2020 took place in Africa, especially East Africa, most likely from wetlands, with strong emissions growth in Canada also. For the year 2020, Qu et al. (2022) attributed 86 ± 18% of the growth surge to increased emissions, especially from wetlands in Africa (15 Tg/yr) and Canada and Alaska (4.8 Tg/yr), although there was also evidence for 14% of the growth coming from a decrease in methane's [OH] sink, to which also Stevenson et al. (2022) attribute part of methane's growth in 2020. Overall, Qu et al. (2022) found total emissions grew by 25–37 Tg/yr in 2019–2020. If their estimate that about 86% of growth was biogenic is accepted, then the growth in biogenic emissions in 2019–2020 was as large as 22–32 Tg.

Drinkwater et al. (2022), over the period 2004–2020, used in situ data to estimate a global annual emission increase of 93 Tg/yr over the period (620 Tg/yr minus 527 Tg/yr), with 83% of that increase occurring since 2011 when the global growth first began to accelerate. Assuming 2.3 Tg/yr/yr of growth is from anthropogenic microbial sources (see Table 2), increased wetland emissions will be responsible for the balance of emissions growth, of 2–2.5 Tg/yr/yr (with very wide uncertainty). Note also that the acceleration of methane's rise from 2020 implies the growth rate of emissions was much higher in 2020–2022.

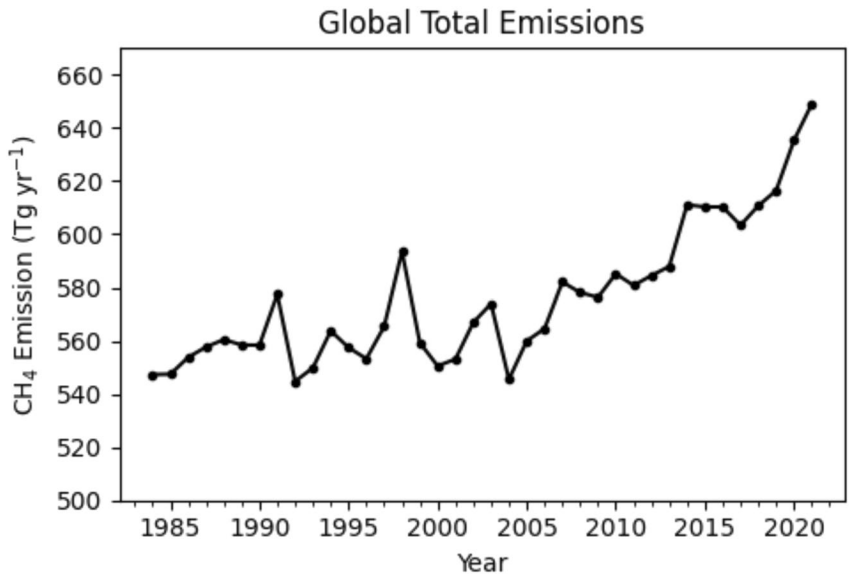

Figure 7. Global methane emissions, estimated and updated using the top-down methodology of Lan, Basu, et al. (2021) and Basu et al. (2022). For further details and data sources, see supplementary information in Lan, Basu, et al., 2021; Figure S2b in Supporting Information S1, red curve, updated.

More broadly, accepting the estimates of Basu et al. (2021) and Qu et al. (2022), and extrapolating to end-2022, a very rough guess is that about 70–80 Tg/yr of the global emission increase between 2006 and end-2022 came from specifically microbial sources, both natural and anthropogenic. As detailed above, microbial emissions from anthropogenic agricultural and waste sources have probably increased between 2006 and 2020 by about 35 Tg/yr (assuming linear growth, Figure 6 and Table 2). If this is correct, the remaining recent net growth in methane emissions is not likely to be primarily attributable to agricultural expansion but has been driven by "natural" biogenic processes, especially wetland feedbacks to climate change.

Figure 7 updates estimated emissions into the 2020s, using the methodology of Lan, Basu, et al. (2021) and Basu et al. (2022). Subtracting (say) 35 Tg for growth over this period in anthropogenic emissions from agriculture and waste, the growth in "natural" biogenic emissions may have been 35–45 Tg. More generally, if total biogenic emissions continue to accelerate at the same rate as in the period 2006–2022 (a very large assumption), then by the year 2037, 30 years after the start of growth, specifically biogenic emissions might have grown by perhaps 100-150 Tg/yr.

7. Glacial Terminations

During the past half-million years, several "termination" events have marked rapid changes of global climate from cold glacial to warmer inter-glacial conditions. Terminations were rapid major reorganizations of the Earth's climate systems, with degassing of upwelling oceans and revival of a warmer biosphere (Broecker & Van Donk, 1970; H. Cheng et al., 2009; Denton et al., 2010; Lang & Wolff, 2011; Raymo, 1997; Schmitt et al., 2012). They are characterized by very large-scale shifts of global and regional weather circulation patterns, for example, from glacial climates toward a more La Niña-like state (H. Cheng et al., 2020).

Broecker and Denton (1990) interpreted "terminations" in the broadest terms, as global-scale climate reorganizations. These were synchronous with sharp changes in the methane burden, likely driven by wetland emissions (Nisbet, 1990; Nisbet & Chappellaz, 2009). The modern paleoclimate understanding of a recognized "Termination", named in Roman numerals from I (youngest) to IX (nearly 800 ka ago) refers to specific transitions from glacial to interglacial periods that took place about every 100 ka. In the finer detail of the glacial record are Dansgaard-Oeschger (D-O) events, which were abrupt warming events, with sharp temperature rises, followed by slow relaxation over millennia. These D-O events were very rapid, with decadal progression (Erhardt et al., 2019). While Dansgaard-Oeschger events occurred within glacials and were likely linked to rapid changes in sea ice cover (Boers et al., 2018), the numbered Terminations marked global-scale climate changes.

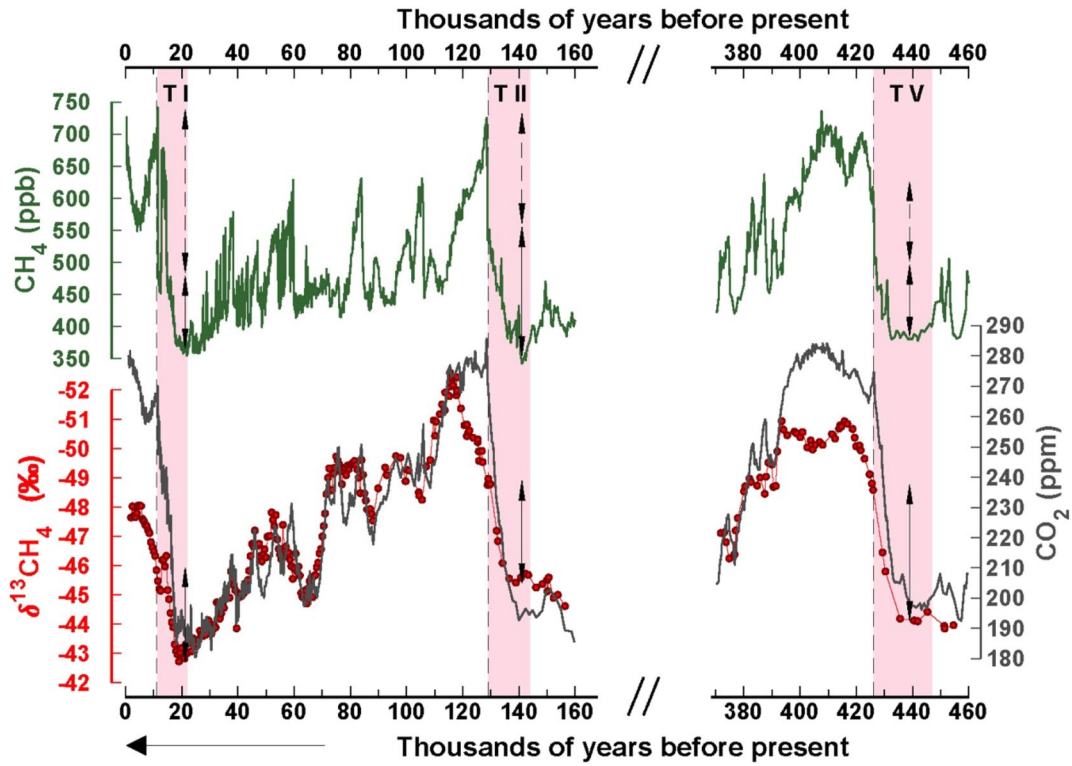

Figure 8. Ice core records from Terminations I, II, and V. Modified from Bock et al. (2017) and updated. Note synchroneity of CH_4 rise with negative shift in $\delta^{13}C_{CH4}$ (plotted upwards on *y*-axis). Solid arrows denote the CH_4 from the start of a Termination to the point of the growth flip. Dashed arrows mark the corresponding CH4 change in the abrupt flip. CO_2 record is from Bereiter et al. (2015) and CH_4 from Loulergue et al. (2008) with updates from Bock et al. (2017).

Although full terminations took several millennia before the new warmer interglacial climate was established, the transitions typically included brief abrupt phases when methane growth and climate warming was very rapid indeed. It is likely that the new warmer weather patterns became established within a few centuries or less (Severinghaus et al., 1998), although it took millennia for the great ice domes to melt and, by their shrinking, to change boreal albedo and replace ice with wetlands and forest, thus completing the full climate transition of the termination.

Sudden methane growth is the bellwether of these changes (Bock et al., 2017; Möller et al., 2013). Methane emissions are very responsive to climate (Nisbet, 1990; Nisbet & Chappellaz, 2009; Petrenko et al., 2009). Methane's growth record during glacial-interglacial Terminations V to I (Figure 8 and Table 3) is preserved in bubbles in ice cores (Bock et al., 2017; Möller et al., 2013; Spahni et al., 2005; Wolff et al., 2009, 2010). The methane record correlates with monsoonal patterns as observed in oxygen isotope records in stalagmites (H. Cheng et al., 2009).

During Termination IA ending the Younger Dryas, methane rose abruptly by ~250 ppb, with essentially synchronous high-latitude and low-latitude climate change (Capron et al., 2021). Ice core data imply emissions increased as much as 6 to 21 Tg/year, causing methane growth rates as high as 6 ppb/yr (Rhodes et al., 2015). It is likely methane's rapid growth was primarily driven by rising tropical emissions, responding to abrupt changes in tropical rainfall (Bock et al., 2017; Möller et al., 2013; Riddell-Young et al., 2023; Schaefer et al., 2006).

Feedback loops in the methane budget rapidly respond to global-scale climate change. It is likely that both warming and climate shifts such as intensification of ENSO events would have especially driven emissions in the tropics where both wetlands and regional land vegetation respond quickly to increased warmth and rainfall, wetland productivity increasing synchronously with expansion of methane-emitting (Clauss et al., 2020; Dutton et al., 2021) populations of ruminants (buffalo, antelope) and pseudo-ruminants (hippoipotamoi).

Figure 8 shows the changes in methane and $\delta^{13}C_{CH4}$ in selected past terminations, showing data updated from Bock et al., 2017; see also Möller et al. (2013). Initially, at the start of a typical termination, there was a gradual rise in methane and CO_2. This rise was accompanied by a negative shift in $\delta^{13}C_{CH4}$, which covaried with CO_2,

Table 3
Synopsis of Termination Changes

Event	Approximate date (ka BP) of abrupt phase	Change over whole termination ppb (approx.)	CH_4 change over whole termination Tg (approx.)	Abrupt phase growth rate ppb/yr (approximate)	$\delta^{13}C_{CH4}$ shift over whole termination (approximate)
PAST					
Termination IA	11.64	250	700	>2.5	−3.5‰
Termination IB	14.65	150	400–450	>2	
Termination II	131	350	900–1,000	>2.5	−4.5‰
Termination III	250	300	800–850		
Termination IV	345	400	1,100		
Termination V	430	350	900–1,000		−5‰
MODERN					
Modern	2006–2023–2037? (Section 9.2 model)	150 up to 2023	374?	~ (Between 6 and 18 ppb)	−0.7‰
			318? (biogenic 85% component)		
Model to 2035	2006 to 2035	573	1,584	10	−1.1‰ (roughly equivalent to −4.4‰ if injected into much smaller glacial burden)

Note. Summarized here from methane records detailed in Section 7, particularly Bock et al. (2017). Assumes 1 ppb is equivalent to 2.77 Tg methane.

as was characteristic during glacials, and with CH_4. This gradual phase lasted a few thousand years.

In typical terminations the brief abrupt phase with its sharp growth in methane by several 100 ppb did not leave a significant imprint in the $\delta^{13}C_{CH4}$ record (Bock et al., 2017; Möller et al., 2013; Schaefer et al., 2006) indicated with arrows in Figure 8. This pattern is consistent with the interpretation that methane emission growth was dominated by equatorial wetland sources which have $\delta^{13}C_{CH4}$ close to the global bulk source (Brownlow et al., 2017; France et al., 2021; Ganesan et al., 2018; MOYA/ZWAMPS Team et al., 2021; Nisbet et al., 2021; Oh et al., 2022). Methane's sharp growth in the abrupt phase is thus best explained by a rapid increase in emissions from tropical wetlands emitting methane with $\delta^{13}C_{CH4}$ close to that of the bulk global source (i.e., especially in the equatorial zone) (Bock et al., 2017).

Switching on tropical wetlands was likely associated with a rapid shift in the ITCZ that coincided with resumption of a strong Atlantic Meridional Overturning Circulation (AMOC) at the start of interglacial climate conditions, initiating a warmer northern hemisphere and generally stable climate with subdued millennial-scale variability. The AMOC "flip" is denoted in Figure 8 by vertical dashed lines, and essentially marked the crux of the termination, although it took millennia for sea level to rise as the great ice domes in Canada and Scandinavia melted. During the "flip" phase, there was typically a rapid increase of about 200 ppb in methane mixing ratio, but only a relatively small change in $\delta^{13}C_{CH4}$.

AMOC changes and consequential meridional heat transport anomalies have been a feature of past episodes of abrupt global climate shifts (W. Cheng et al., 2007). For example, Riveiros et al. (2013), and Rhodes et al. (2015) showed that AMOC slowdown is capable of producing atmospheric responses that extend throughout the Northern Hemisphere and into the tropics, with strong coupling between the two regions. Though very different from today's changes, the 32 ppb rise in atmospheric methane during the HS 1 event reported by Rhodes et al. (2015) has interesting parallels with modern shifts, including both weakening of AMOC and southern expansion of the ITCZ and Hadley cell. However, there are also large differences: in HS1 there was boreal cooling as the ITCZ moved southward; in the present event the north is warming strongly.

Although there are many possible explanations of this sequence of events, the pattern is consistent with a wider scenario beginning with initial modest Hadley cell expansion during interdecadal variation, bringing about more methane emission from wetter outer tropical swamps ($\delta^{13}C_{CH4}$ perhaps very roughly −60‰ in cool conditions compared to today). Then in response, changes in AMOC, the Walker circulation and the Indian Ocean Dipole (IOD) (Abram et al., 2020; Brierley et al., 2023), may have brought about intensification of equatorial rainfall and consequent rapid growth in equatorial wetland emissions, initiating methane's abrupt rise.

Thus in this scenario of the abrupt phase of a glacial termination, the growth of wetlands under strong equatorial rainfall will rapidly increase the atmospheric methane burden but be accompanied by only subdued initial leverage on $\delta^{13}C_{CH4}$. Then, as the boreal realm warms, northern methane sources with more negative $\delta^{13}C_{CH4}$ begin to contribute. Note that in an end-glacial scenario the presence of large ice domes over Canada and Scandinavia inhibited development of boreal vegetation: in these areas boreal wetlands were not functioning until millennia later when the ice melted. Today, the boreal and Arctic wetlands, which emit methane with markedly negative $\delta^{13}C_{CH4}$, are very productive and are experiencing strong warming (Previdi et al., 2021).

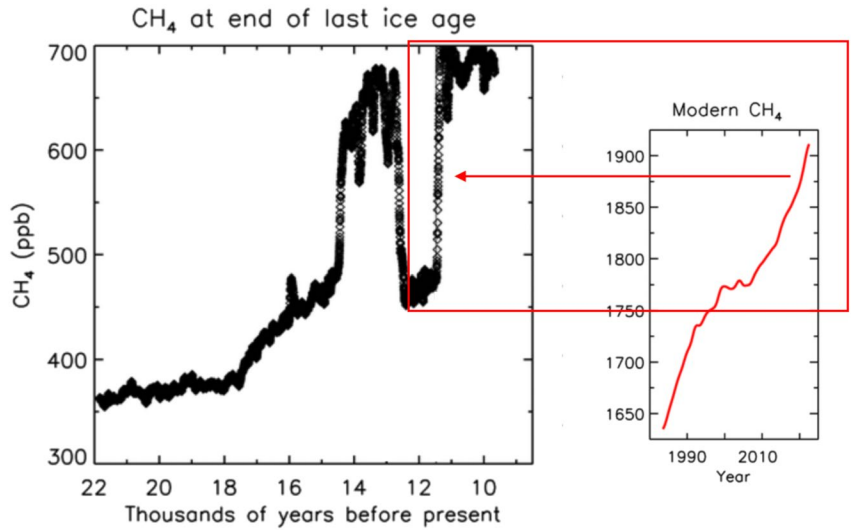

Figure 9. Comparison between Methane's record during Termination 1 and methane's growth since 1980s. Note—these plots are not to the same time scale. (Left panel) Methane record during Termination 1 from references cited in text. Prior to about 17 ka before the present, methane was below 400 ppb (from various sources: see text). Methane rose in Termination IB, especially in the abrupt phase about 14.65 kyr ago. The Younger Dryas. 12 ka ago, saw a return to cold conditions, especially in the northern North Atlantic, abruptly ended in Termination IA, 11.64 kyr ago, date shown by vertical climb. (Right panel) Modern methane record. Growth prior to 2006 shows convex equilibration trend; growth from 2006 shows concave (accelerating) trend. Note time scales not the same. NOAA data (https://gml.noaa.gov/aftp/data/trace_gases/ch4c13/flask/surface/).

Over full terminations, negative drops in $\delta^{13}C_{CH4}$ ranged between −5‰ and −3‰ (Bock et al., 2017). For example, in Termination V, $\delta^{13}C_{CH4}$ dropped from about −44‰ to −49‰, while in Termination II there was a similar negative shift (Bock et al., 2017). Again, at the start of the Preboreal Holocene $\delta^{13}C_{CH4}$ shifted from about −43‰ in full glacial conditions, to about −46.3‰ (Bock et al., 2017; Fischer et al., 2008; Melton et al., 2012).

To consider the older events first, the abrupt phase of Termination II took place between 130.9 ± 0.9 and 130.7 ± 0.9 ka ago (Moseley et al., 2015), with contemporary strengthening of the monsoon. In Terminations II and III the methane burden rose by roughly 500–600 Tg in sudden growth events. During similar abrupt rises in Terminations IV and V, methane rose from about 400 to 700 ppb, or more, increasing the methane burden by 800–900 Tg.

The most recent termination was in multiple phases (Figure 9 left panel). In the abrupt part of Termination 1B, which ended the last major glaciation, the Greenland Summit climate rapidly warmed by 9 ± 3°C, and 20–30 years later methane rose abruptly (Severinghaus & Brook, 1999). Methane rose quickly over the 60 years between 14655 and 14595 BP, with especially rapid growth in the decade from 14655–14645 BP (Severinghaus & Brook, 1999). This change initiated the Bølling–Allerød interstadial, until 12.87 thousand years BP, when the Younger Dryas began, with sudden cooling of the North Atlantic realm linked to a drop in methane to 450–500 ppb. Then, ending the Younger Dryas, the abrupt warming event of Termination 1A took place between ∼11700 and 11610 BP, with the fastest change about 11.64 thousand years ago (indicated by vertical line in Figure 8). About 0–30 years after this warming began, methane rose sharply to above 700 ppb (H. Cheng et al., 2020; Severinghaus et al., 1998). In all, methane rose as much as 250 ppb in little over a century, an increase of about 700 Tg in the burden.

There is evidence for strong growth in "tropical" (taken here as 30°S to 30°N) methane emissions during Termination 1 (Baumgartner et al., 2012; Riddell-Young et al., 2023), as tropical wetlands responded to an abrupt expansion of tropical rain belts. Methane output may have risen from perhaps 60 Tg/yr during glaciation to 120 Tg/yr or more in the post-termination Holocene. That global increase of 60 Tg across the whole event can be compared to the present-day conservative estimate derived above that "natural emissions" have increased by about 35–45 Tg since 2006. Riddell-Young et al. (2023) and Baumgartner et al. (2012) also found evidence for a supplementary role of emissions from boreal methane sources, findings prescient of the present-day results of Qu et al. (2022). Similar patterns are also inferred from the weak interpolar gradient for methane in Termination 1B which suggests methane growth was driven by a major tropical input (Severinghaus & Brook, 1999).

In addition to termination events, examples of rapid changes in atmospheric methane, in which methane rose by 32–53 ppb, are also recorded in Heinrich events during glacial periods. Though not analogous to present-day conditions, the rapid methane changes are instructive as they show how responsive methane emissions are to climate shifts. Heinrich events are marked by layers of ice-rafted debris in the North Atlantic seabed record, that must have been dropped by armadas of icebergs breaking off the ice sheets over Greenland and North America. Studying the HS1 event (16.15 kyr BP), which occurred near the end of the last major glacial period, Rhodes et al. (2015) inferred a marked southerly shift in the ITCZ had taken place in response to Northern Hemisphere cooling and greater sea-ice cover, causing a major expansion in southern hemisphere wetlands, which in turn drove a rapid increase in methane emissions by 29 Tg/yr.

To conclude, the methane and $\delta^{13}C_{CH4}$ records of glacial/interglacial events are consistent with the hypothesis that the abrupt phase of methane growth was driven by a very rapid biogenic response, mainly from tropical wetlands.

8. Meteorological Changes

Meteorologically, past termination events may have originated in specific regional locations and then spread globally. For example, in the North Atlantic realm, the rapid meteorological changes in the most studied abrupt termination event, the end of the Younger Dryas (T1A), may have been a consequence of a set of changes originating in the tropics and then spreading to include the North Atlantic, the Asian Monsoon and the Westerlies (H. Cheng et al., 2020). Moreover, model experiments typically show a spin-up time before any change has impact on the global methane budget: thus for a methane signal to have become identifiable in the period 2007–2022, the changes triggering the necessary spin up would have been perhaps a decade or more ago.

If the post-2006 methane growth represents more than multi-decadal variability and is indeed the start of a major long-term reorganization of the planetary climate system, then two questions arise: Can such global-scale modern meteorological changes be identified, given that both short-term change and sustained regional multi-decadal variability are characteristic of the Holocene climate (Wanner et al., 2008)? Are there today any direct signs of incipient global-scale meteorological reorganization?

Recent meteorological changes, though different in style and regional impact, may indeed be similar in speed and planetary scale to global changes during termination events. During 2006–2020 the total Earth system has experienced a remarkable heating imbalance of 0.76 ± 0.2 Wm^{-2} with about 89% of the heat stored in the ocean, 6% on land, 4% in the cryosphere and 1% in the atmosphere (von Schuckmann et al., 2023). Even a small increase in the partitioning of this heat into the air will have dramatic impact on global weather.

Strong global-scale evidence for dramatic present-day climate warming comes from the heat content of the upper part of the oceans (von Schuckmann et al., 2023), which not only has a sustained and strong warming trend, but the rate of warming is accelerating (L. J. Cheng et al., 2023). Warming has been particularly anomalous in the South Atlantic, in the North Atlantic offshore North America and in the Indian Ocean offshore Southern Africa. Ocean heat produces evaporation and thus precipitation: wetlands will respond. The "triple-dip" La Niña of the first years of this decade must be a factor (McPhaden et al., 2023), while multi-centennial variability of internal origin may also be important.

In recent years, there has been marked weakening of the Atlantic Meridional Overturning Circulation (AMOC), in particular since 2005 (Bonnet et al., 2021; Ditlevsen & Ditlevsen, 2023; WMO, 2023). Concurrently, changes in the Walker circulation (El Niño/Southern Oscillation, ENSO) and the Indian Ocean Dipole (IOD) have had profound impacts on tropical precipitation and temperature on land. Hadley cell expansion has shifted the zone of tropical cyclones (Sharmila & Walsh, 2018), with poleward shifts in extra-tropical storm tracks and jets, and upper tropospheric warming. As during glacial/interglacial transitions, and particularly in the abrupt "flip" phase, the Hadley circulation is expanding again today and the extension of the subtropical edge of the Hadley circulation has already had impact on a wide range of extratropical biological productivity (e.g., Osland et al., 2021; Pandey et al., 2017). These poleward shifts of the planetary circulation and the concurrent expansion of tropical weather systems are now becoming well-documented (Grise et al., 2019; Staten et al., 2020; Studholme et al., 2022; Voigt et al., 2021).

Tropical weather systems are tightly interlinked (Cai et al., 2019; McPhaden et al., 2023), with widespread major recent changes. Geng et al. (2022) have suggested that increased ENSO changes may emerge much sooner than hitherto expected, while B. Wang et al. (2019) presented evidence for major shifts in the origina-

tion and strength of El Niño events, finding more frequent occurrence of extreme events since the 1970s and changes in ENSO onset from originating in the eastern Pacific to the western Pacific. McPhaden et al. (2023), Hasan et al. (2022), and Jo et al. (2022) suggested linkage between the IOD and Atlantic and Pacific conditions. Sun et al. (2022) present evidence for substantial increases in early onset of monsoon weather and positive IOD events, with dramatic impacts on regional flooding. In particular, rains in central and eastern Africa have strong links to the IOD and ENSO cycles, and are dependent on changes in the Walker circulation (Nicholson, 2015) together with the strength and timing of pulses of the Madden-Julien oscillation. Catastrophic rains and floods in East Africa in 2019 came from a remarkable concatenation of meteorological factors, including record levels of the Dipole Mode Index, ENSO effects, anomalous zonal winds over the central Indian Ocean, very warm sea surface temperatures in the eastern Atlantic and Indian Oceans, and unusual zonal circulation (Nicholson et al., 2022).

These recent large-scale shifts in the IOD and unusual ENSO changes (Pandey et al., 2017) have profound impacts on methane emissions. Feng et al. (2022) attributed much of the change in methane emissions over tropical South America and tropical Africa to IOD and ENSO shifts. Dramatic changes may be affecting the IOD, which plays a major role in controlling rainfall over the wetlands of east sub-Saharan Africa (Feng et al., 2022), with recent trends toward more frequent and intense positive events (Abram et al., 2020). During strong La Niña episodes, rainfall can deeply fill wetlands, while during El Niño episodes various parts of Amazonia and East Africa have experienced changes likely related to climate warming, with longer dry- and shorter wet-seasons in some places, and fires spreading to areas that have not burned for millennia; the opposite taking place in other regions.

Polar climates are also changing rapidly (Łupikasza & Cielecka-Nowak, 2020) especially with Arctic amplification of warming (Previdi et al., 2021). Arctic sea ice is in very rapid retreat (Kim et al., 2023). Arctic amplification may be linked to a negative Northern Hemisphere Annular Mode, large scale circulation changes, and increased durations of weather patterns and extreme precipitation over the Northern Hemisphere (Liu et al., 2021). Weather patterns are shifting in continental interiors (IPCC, 2021 their Figure 8.11), with regional warming across Siberia (P. Wang et al., 2022). Regional climate warming has had significant impact on plant productivity, promoting the greening of the tundra (Berner et al., 2020). Boreal and Arctic warming have had marked effects on temperature and precipitation over large swampy areas, for example, in western Siberia (Gorbatenko et al., 2020), presumably by increasing supplies of organic detritus and thus methanogen productivity.

These profound ongoing global-scale changes in the modern ocean and atmospheric circulation patterns have many parallels in past termination events (see Section 7 and Figure 8), though with the caveat that the modern world is profoundly different, especially in the absence of the major meteorological impacts of the large ice domes over Canada and Scandinavia. Thus any global-scale meteorological changes that occur in the next few decades will clearly be very different from the glacial/interglacial transitions. Yet perhaps there are analogies too, particularly in the paleoclimatological evidence that the global climate system can reorganize very rapidly indeed, over as short a time period as a few decades.

A further caveat: although the present-day meteorological changes are widespread and profound, clearly on an inter-hemispheric scale, and likely involving multiple interlinked teleconnections, they may yet still be within the multi-decadal or centennial spectrum of Holocene variability. Many major meteorological circulation patterns have only recently been identified and their record of change compared to the recent historic past remains poorly documented, although the IPCC (2021) Summary for Policymakers commented that evidence of observed change has strengthened since the previous assessment report. It is not clear that current climate extremes, though large, abrupt, and ongoing, and with potent impact on methane emissions (Feng et al., 2022), are great enough in sum to be evidence for an ongoing global-scale meteorological reorganization. A grand-scale meteorological progression of the type identified by H. Cheng et al. (2020) would be hard to identify from weather data while it took place, and likely only recognizable in retrospect. The evidence remains unclear.

Moreover, apart from the measurement of heat stored in the oceans (L. J. Cheng et al., 2023; von Schuckmann et al., 2023), it is difficult to quantify the total sum of change, nor to quantify the collective impact on global climate. But equally it is plausible that the multiplicity of recent events, their abruptness, and their power are circumstantial signs a major reorganization of the global climate system has already begun. Like the heat of the oceans, the biogenic methane signal may be a telling summation, a bellwether that signals the onset of permanent global change, the end of the Holocene.

To summarize the results in Sections 1-8: In the period 2007–2022, methane's growth rate has been very high, with an overall concave (accelerating) trend and a significant negative shift in $\delta^{13}C_{CH4}$. If the estimates given above of the growth in agricultural emission are accepted, then much of the new emissions that are driving this growth come from wetlands and other natural sources, as found by Basu et al. (2022), Qu et al. (2022), Feng et al. (2022, 2023), Peng et al. (2022), and Rosentreter et al. (2021). If the "85% biogenic" estimate (Basu et al., 2022) continued to apply in the year 2021, growth from specifically biogenic emissions in that year alone (i.e., growth from climate change feedbacks, both wetland and agricultural and waste) may have been 15 ppb, implying the present-day "non-fossil fuel" growth trend by itself is very significantly faster than the abrupt phase growth rates in the ice core records (Table 2).

9. Modeling

9.1. Modeling Methodology

Is methane's growth since late 2006 now becoming comparable in scale and in cause to methane's growth during a termination event?

To address this question, modeling focused on the question: what would happen to the methane burden and its $\delta^{13}C_{CH4}$ during the abrupt phase of a termination event, if the abrupt growth took place today? This is not a model to replicate the paleoclimate record but to elucidate modern trends. Thus the model is set up with a modern distribution of wetlands, including both tropical and boreal wetlands (which were largely absent in glacial periods). The model is designed to match century-scale trends over a conceptual abrupt growth phase of 30 years, and to follow major emission variations over this period.

A modified version of the model used in Nisbet et al. (2019) was used. The model is a running budget model with four semi-hemispheres and exchange rates between them consistent with the observed interhemispheric rate of mixing. Methane removal uses [OH] destruction from Spivakovsky et al. (2000) with kinetic isotope exchange from Cantrell et al. (1990), Cl removal from Hossaini et al. (2016), and soil removal from Curry (2007). The model was designed to examine changes in methane mole fraction and in methane's isotopic content, averaged over four semi-hemispheric regions (30–90°S, 0–30°S, 0–30°N, and 30–90°N), with exchange rates between them consistent with the interhemispheric transport time. Fitting methane's carbon isotopic record is central to the modeling because of the powerful insights $\delta^{13}C_{CH4}$ provides into changing methane sources (Craig et al., 1988).

We first modeled an abrupt ("flip") phase patterned on the abrupt phase of a "typical" termination event, to understand its dynamics. Then, having characterized the abrupt phase of a typical event, we used the model to match the current (21st century) growth record. The model tracks the impact of a sharp increase in biogenic methane, to test whether it is comparable to the sudden changes in a typical termination.

9.1.1. "Source Jump" Termination Event Model—Changes in Methane Burden and $\delta^{13}C_{CH4}$

We simulated modern-type emissions growing over a time period of 30 years, into a putative model of methane's glacial-like atmospheric burden to see if a "termination-like" pattern developed, not just replicating the growth in methane burden but also to investigate the $\delta^{13}C_{CH4}$ isotopic consequences.

Biogenic sources used in each semi-hemisphere for the "Ice-age" and "Termination 1" periods are scaled down from a modern scenario fitting recent CH_4 and $\delta^{13}C_{CH4}$ data (Nisbet et al., 2019) and are not from glacial-period biosphere reconstructions, but the fossil fuel contribution, taken as 30% of the total source at present (Lassey et al., 2007; Lowe et al., 1988), was omitted. Relative to the total, the distribution of CH_4 sources by semi-hemisphere was: 12.4% in 30–90°S (HSH); 27.7% in 0–30°S (LSH); 31.1% in 0–30°N (LNH); and 28.8% in 30–90°N (HNH). The analysis of geographic spread was not expected to be very sensitive to the latitudinal distribution of fossil methane sources but the omitted recent fossil fraction was taken as being distributed 20%:40%:40% in LSH:LNH:HNH. Omitting the fossil fuel emissions source leaves a distribution for the other sources as: 17.7% in HSH; 31.0% in LSH; 27.3% in LNH; and 24.0% in HNH.

These proportions according to latitudinal zone applied to a global total source consistent with sources scaled to give a global mean CH_4 mixing ratio of 700 ppb for "post-transition" and 400 ppb for "initial" conditions. The initial scenario also reduced the 30–90°N (HNH) region source further because cold temperatures restrict land plants and especially wetland areas and productivity. Global average results are not particularly sensitive to

Table 4
Source Emissions, $\delta^{13}C_S$, Mixing Ratios and Atmospheric $\delta^{13}C_M$ in Modeled "Initial" (Pre-Transition) to Post-Transition ("Post") Values

	Source Tg/yr (running annual average)					Source $\delta^{13}C_S$ ‰				
	30°S–90°S	0°S–30°S	0°N–30°N	30–°N90°N	Global	30°S–90°S	0°S–30°S	0°N–30°N	30°N–90°N	Global
Initial	23.6	46.7	41.8	21.4	133.5	−49.8	−50.8	−51.7	−56.4	−51.8
Post	30.9	78.2	79.6	45.1	233.7	−53.8	−54.3	−54.8	−57.5	−55.0
	Mixing ratio ppb (running annual average)					Atmospheric $\delta^{13}C_M$ ‰				
	30°S–90°S	0°S–30°S	0°N–30°N	30°N–90°N	Global	30°S–90°S	0°S–30°S	0°N–30°N	30°N–90°N	Global
Initial	408.6	403.5	396.7	393.8	400.7	−44.7	−44.7	−44.7	−44.82	−44.75
Post	694.2	695.1	698.9	699.9	697.0	−47.9	−47.9	−48.0	−48.0	−48.0

Note. Derived from data in Bock et al., 2017 and other cited references.

how much the HNH region is reduced relative to the global total source, but results are shown for the HNH region source being reduced from 24% to 16% of the total with the other 8% distributed equally over LNH and LSH.

The isotopic signatures of the "Initial" (i.e., pre-transition) sources (S), here termed $\delta^{13}C_S$, are taken as having $\delta^{13}C_S$ 4‰ heavier than present sources, and the source pulse of increased emission leading into the transition is taken as having $\delta^{13}C_S = -59$‰, a value typical of modern outer (seasonal) tropical wetlands (France et al., 2021; MOYA/ZWAMPS Team et al., 2021). The transition between the "pre-transition" and "post-transition" states of the global methane budget is done with a constant rate of change in the source, and its $\delta^{13}C_{CH4}$, over 30 years. Mixing ratio, source emissions, *Src* (Tg/yr), source signatures for $\delta^{13}C_S$, and atmospheric $\delta^{13}C_{CH4}$, here termed $\delta^{13}C_M$, are summarized in Table 4.

9.1.2. Modeling Results

Plots of the changes in methane mixing ratio and $\delta^{13}C_{CH4}$ in the modeled *"Source jump" Scenario* (Table 4), are shown in Figures 10a and 10b. This sequence of events is broadly similar to the real records of the methane burden in typical glacial terminations. The isotopic results reflect the very rapid growth of emissions from all latitude zones, both tropical and boreal. The isotopic results show the "Tans effect" (Tans, 1997), with changes in $\delta^{13}C_M$ overshooting followed by a slow recovery—that is, with $\delta^{13}C_M$ taking longer to equilibrate than the mixing ratio. Inter-hemispheric spatial gradients take time to adjust after major changes in emissions and Tans (1997) pointed out that the timescale for the $\delta^{13}C_{CH4}$ ratio is also longer than for methane's abundance so provides complementary information.

In actual glacial terminations, the boreal wetlands took longer to deglaciate and hence the dominance of tropical emissions with $\delta^{13}C_{CH4}$ close to the bulk atmospheric source led to a brief hiatus in $\delta^{13}C_{CH4}$ while the burden grew. In the model, unlike the real past record, the abrupt growth of boreal sources produces a significant negative shift in $\delta^{13}C_{CH4}$.

9.2. Present-Day Scenario: Modeling Methane's Modern Growth and Predicting the Near Future

To predict the impact if current trends continue for a full model span of 30 years, from end-2006 to 2037, the second model experiment focused on matching the current growth in methane emissions and then projecting into the future until the change is assumed to be completed after 2036. This is an optimistic scenario that assumes good progress in the Global Methane Pledge to reduce methane emissions from purely abiogenic (fossil fuel) sources, and that biogenic emission growth then slows in a stable future climate.

9.2.1. Modern Event Methane Growth Model—Changes in Methane Burden and $\delta^{13}C_{CH4}$

The "modern-day" model run is for a 30-year period 2007–2037, together with initializing years and years of post-change stability in emissions budgets. After the 30-year period, emissions stabilize. In this model, sources are fitted to observations with a simple piecewise linear fit of both source emissions, *Src* (Tg/yr) and $\delta^{13}C_S$ up to 2022 (Figure 11). Then the projections in Figures 11a and 11b that go beyond 2022 extend the source flux growth that was fitted to the most recent data, and continue for the rest of a 30 year transition period. The isotopic signature $\delta^{13}C_S$ is determined by assigning a constant $\delta^{13}C$ lighter than the current average $\delta^{13}C_S$ to the *Src* increase.

For the *Present-day Scenario*, Figure 12a shows NOAA methane mixing ratio and atmospheric $\delta^{13}C_{CH4}$ data together with an extrapolated extension of the running budget analysis in Nisbet et al. (2019). The fit-to-data follows a smoothed version of the observed mixing ratio, shown in Figure 12a, with a maximum growth of 14.5 ppb/yr in 2022 (Figure 12b), when the observed rate was actually similar, following an 18 ppb rise in 2021. This fit-to-data is up to August 2022 for the observed mixing ratio and $\delta^{13}C_{CH4}$ measurements, and then extrapolated to 2037, for a full 30-year period of emissions growth. The scenario has an overall mean growth rate over 30 years of 10.5 ppb/yr.

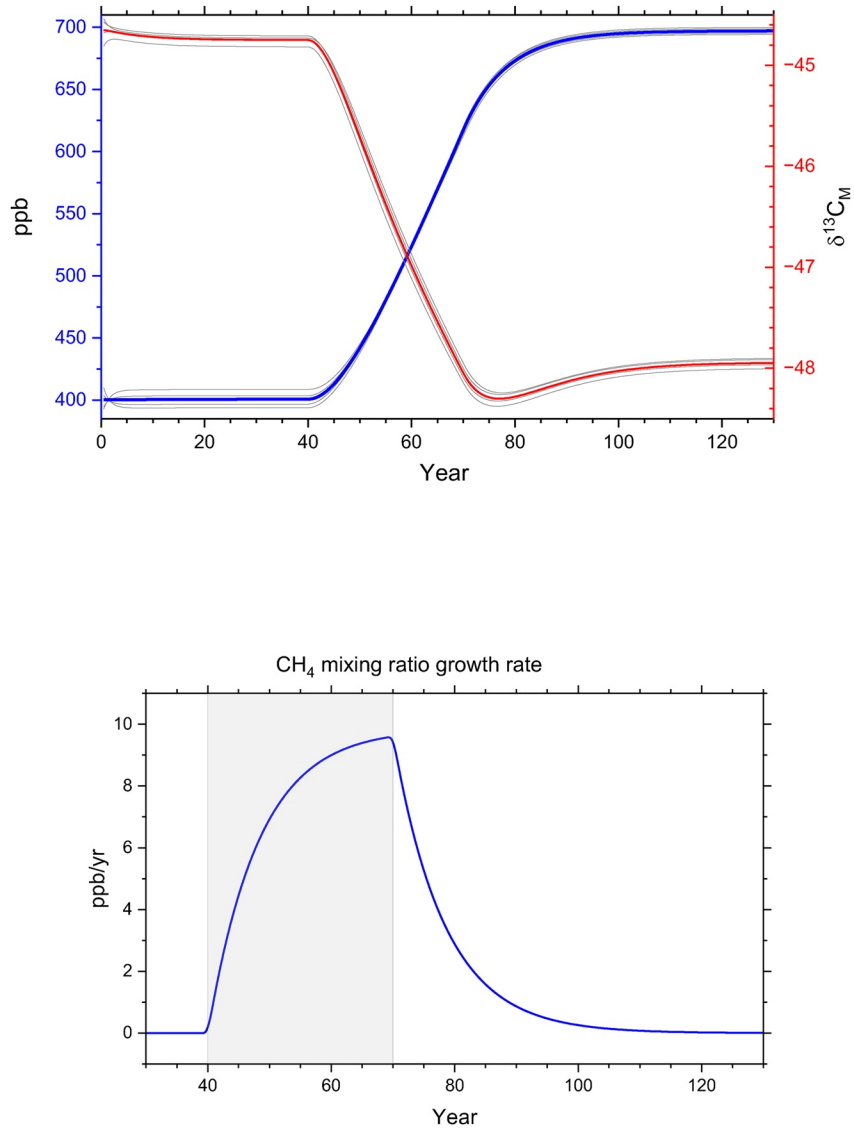

Figure 10. Termination event model (Section 9.1.1) (a) Methane mole fraction ($\delta^{13}C_M$) in ppb and $\delta^{13}C_{CH4}$ from the 4-box running budget analysis with a 30-yr transition from "Initial" to "Post" sources. Blue is the global average mole fraction and thin lines are for the four semihemispheres. The latitudinal distribution of the CH_4 mole fraction reverses from being lowest in 30°N–90°N to being the highest there. Red is the global average $\delta^{13}C_M$ and thin lines show values for each semihemisphere and this change in $\delta^{13}C_{CH4}$ is uniform across all semihemispheres. (b) Growth rate (ppb/yr) of the global average CH_4 mixing ratio in Figure 10a.

This analysis successfully tracks the observed inflexion and then decrease in atmospheric $\delta^{13}C_{CH4}$ (see Figure 4 and green circles on red curve in Figure 12a), observed until 2022. In the projection part of the model analysis, the global mean CH_4 mixing ratio reaches 2348 ppb and stabilizes around the year 2055. The budget analysis also follows the observed decrease in $\delta^{13}C_M$, which reaches a minimum in the year 2040 followed by some recovery. Stabilization of $\delta^{13}C_M$ takes longer than for the mixing ratio because of the Tans effect, with $\delta^{13}C_{CH4}$ eventually reaching a minimum in 2040, followed by some limited recovery as the burden equilibrates, while the global mean $\delta^{13}C_s$ of source emissions decreases from −54.3‰ in 2006 to −55.2‰ in 2099.

Our modeling suggests that the modern pulse of new biogenic methane, despite ongoing anthropogenic fossil fuel inputs with relatively positive $\delta^{13}C_{CH4}$, is capable of shifting the $\delta^{13}C_{CH4}$ of the much larger whole modern atmospheric burden by, say, −1.1‰ over the full 30 year period 2007–2037. That includes inputs of equatorial methane with little isotopic leverage, outer seasonal tropical methane with some isotopic leverage, and boreal/Arctic meth-

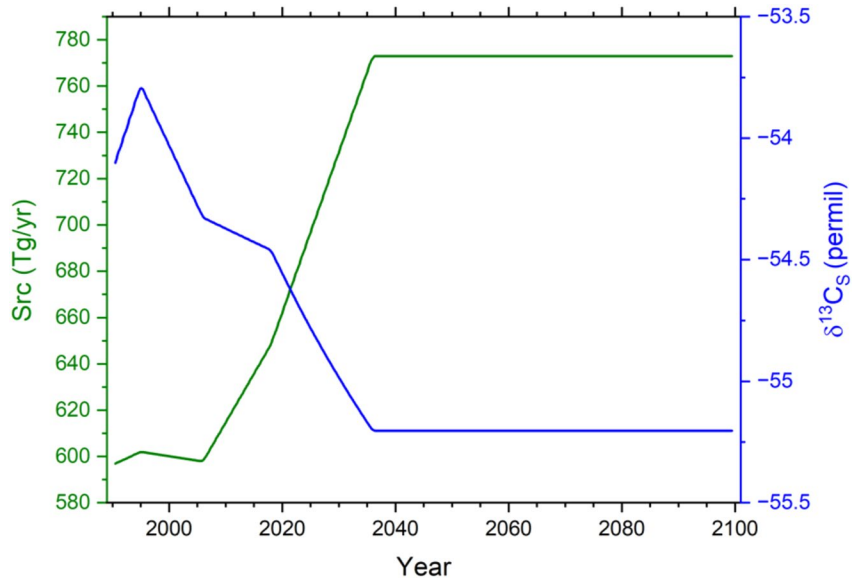

Figure 11. "Modern-day" model for a 30 year transition period 2007–2037 assuming a change from earlier global climate state ending in late 2006 to new stable climate state beginning in 2037. Source flux (Src) and source isotopic signature $\delta^{13}C_s$ modeled to fit to measurement data (see the image) up to 2022, thereafter projected to end of 30 year period, after which Src and $\delta^{13}C_S$ remain constant.

ane with strong isotopic leverage. In the real record of the contemporary modern atmosphere, prior to the onset of growth in 2006, the mean atmospheric methane burden was slightly over 4,900 Tg. In 2022, the mean burden had risen to 5,300 Tg, a net increase of roughly 400 Tg during 2006–2022 inclusive. The accompanying $\delta^{13}C_{CH4}$ shift of about −0.55‰ includes a "positive" isotopic input from thermogenic sources such as anthropogenic fossil fuel emissions and biomass burning with isotopic signatures more ^{13}C rich than the bulk atmospheric source. Had there been no such positive leverage, the total biogenic-driven $\delta^{13}C_{CH4}$ shift over 2007–2022 that we would now be measuring would have been perhaps −0.7‰. Note that this shift has occurred despite the new emissions being diluted into a global burden five times larger than in glacial periods. A comparable pulse into the glacial air would shift $\delta^{13}C_{CH4}$ negative by 3–4‰ over a complete termination, including turn-on of boreal sources.

To conclude: If methane emissions, primarily from biogenic methane sources, continue to rise at a rate similar to the one observed in recent years, the modern rise since 2006 would be large enough to be identified as the first part of a "termination-scale" event in the ice core record of atmospheric methane. The conclusion also holds if only 85% of the current growth is considered, given that 15% of the ongoing rise is likely from fossil emissions that may be mitigated in the near future. Even if livestock emissions growth as fast as 1.4 Tg/yr/yr (L. Zhang et al., 2022: see above) is deducted, the remaining "non-fossil fuel, non-livestock" growth rate still bears comparison with abrupt growth in a termination-scale event, the more so because the methane productivity of tropical livestock, like the wild ruminants they have replaced, depends on vegetation growth that in turn follows climate-driven rain and warmth.

10. Discussion of Comparison

To summarize, methane's mole fraction growth in the past 15 years is comparable to growth in termination events, and it is likely that ongoing changes in methane emissions from present day wetlands are comparable to feedbacks during past global change events. Even if only 85% of modern methane growth is biogenic, and part of that biogenic growth is due to anthropogenic inputs like increased cattle populations and more use of nitrogen fertilizers, methane's non-anthropogenic growth in the past 15 years has been at least comparable to growth in past climate change events. Allowing for the difference in the mass of the pre-transition burden, the associated isotopic shift is also comparable to shifts recorded (Figure 8) across whole termination events (i.e., after the boreal wetlands had become fully active).

It remains unclear how much the biogenic changes to the methane budget in recent decades are within the natural range of responses to decadal or centennial-scale climate variability.

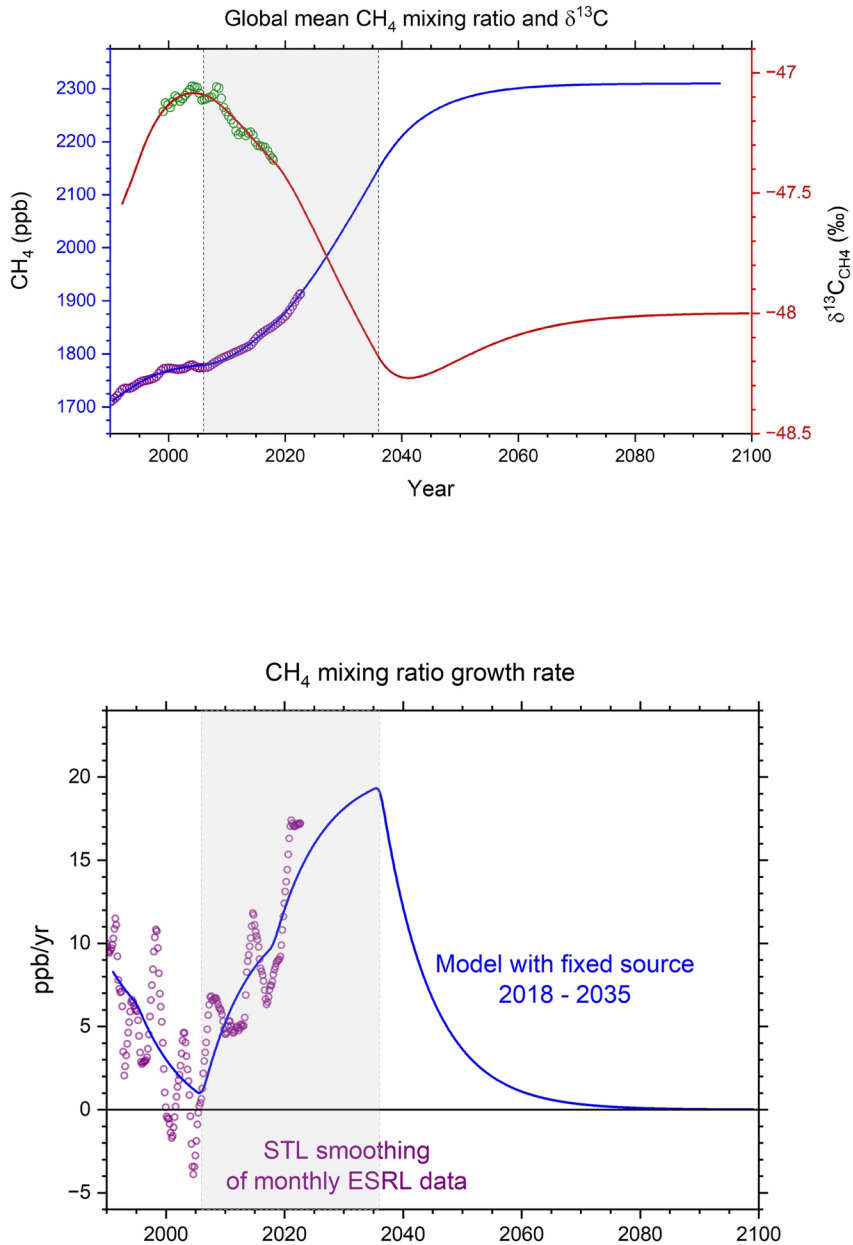

Figure 12. (a) Change in global mean mixing ratio (blue) and $\delta^{13}C_{CH4}$ (red) together with NOAA data to August 2022 and $\delta^{13}C_M$ data (green) to 2018. Compare with Figure 10a. (b). Observed methane growth rate in ppb/yr from the NOAA data and from the model using a fixed source strength up to 2037, as shown in Figure 11. The measurement-based growth rate determination uses the Seasonal Trend Loess analysis of Cleveland et al. (1990) to separate a changing seasonal cycle from a changing trend. Compare with Figure 10b. NOAA data from https://gml.noaa.gov/aftp/data/trace_gases/ch4c13/flask/surface/.

The current methane growth event started in late 2006 in both northern and southern high latitudes (Figure 13). In Arctic summer, southerly winds blew high-methane air poleward from boreal zones. From then on, the tropics became the main zone of methane growth, especially in 2014/2015, but with marked growth in the northern temperate zone in 2014 and in the southern outer tropics around in 2018 (e.g., Pantanal wetland). Then came the extraordinary ongoing growth surge of 2019–2022. The sine-latitude-time methane map in Figure 13 (updated from Lan, Nisbet, et al., 2021) reflects this history, though with the obvious caveat that changes in natural sources and sinks are added to by changes in human emissions from the fossil fuel industry, agriculture and waste.

Although the ongoing increase in global biogenic methane emission might be within the multi-century range of historic emissions variability (Figure 3) (Ferretti et al., 2005; Mischler et al., 2009), the speed-of-change of the

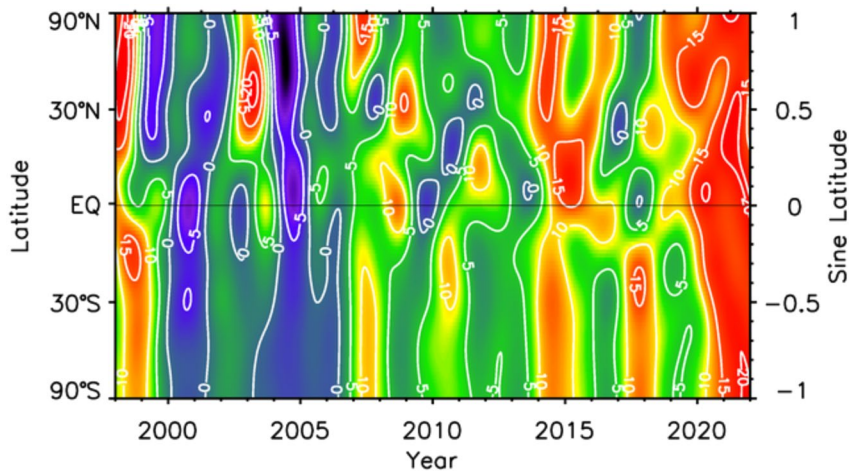

Figure 13. Methane growth rate averaged by latitudinal zone, from 2000 through 2021, updated from NOAA data. Red "warm" colors—growth. Blue "cool" colors—decline. The vertical axis denotes the sine of latitude, which weights each latitude band by its atmospheric mass. The Inter-Tropical Convergence Zone migrates seasonally from roughly 30°N to 30°S (sine latitude 0.5 to −0.5), while the Arctic zone is the band north of sine latitude 0.91. The current growth event began in late 2006. Note the remarkable growth since 2020. Data from https://gml.noaa.gov/aftp/data/trace_gases/ch4c13/flask/surface/.

modern trend is extreme, much more rapid than methane's medieval changes or the post-1800 rise driven by fossil fuel use. The inference is that the biogenic component of methane's current (2007–2022) change is indeed likely outside the range of natural variability.

Methane's modern growth, in ppb/yr, and isotopic shift are more rapid than in glacial-interglacial terminations (Table 3), though not necessarily faster than the maximum decadal change rates during some terminations. Thus there is evident similarity between the past increases in tropical biogenic sources that drove the glacial-interglacial terminations and the present-day biogenic inputs driving the current 2006–2022 rise in methane emissions. Though the events are very different, in the 15 years of growth to date the modern rise does indeed bear comparison with the scale and speed of the abrupt phase of a termination event.

Previous orbitally driven natural transitions from cold glacial periods to warmer interglacial periods took place in the presence of large ice caps and widespread sea ice. In contrast, the modern climate change is from a warm Holocene (i.e., with widespread northern wetlands) to a new, presumably even warmer future. The comparison between modern growth and past analogs should not be taken too far. A modern "termination-style" event marking the reorganization from a Holocene warm climate to some new post-Holocene yet-warmer climate will be very different from any of the end-glacial events of the past half-million years.

Moreover, today's transition is anthropogenically driven, in an atmosphere where CO_2 is much higher and rapidly growing, and where crop wastes and fertilizer run-off are widespread. Thus it may be that the wetland response today has already surpassed the wetland response in past glacial interglacial terminations.

Yet it is indeed possible to imagine a new, modern step-change reorganization of the planetary climate in a global "termination-scale" event—this could include marked ocean warming and expansion of the ITCZ, and changes in the behavior of the IOD as the Hadley circulation expands coupled with alteration in the strength and frequency of ENSO variations. Such changes could be accompanied by rapid Arctic land-surface warming and sustained ocean circulation responses, including changes in the AMOC, on centennial-level timescales (Matsumoto, 2007).

Compared to the "natural" CO_2 budget, which has a major component in the deciduous vegetation of the temperate northern hemisphere, changes in the biogenic methane signal reflect methane's more global distribution of sources and sinks. In past paleoclimate transitions, large changes occurred in the CO_2 budget, in response to changing latitude distribution of insolation or meteorology and warming oceans. But such feedback-related changes in CO_2 are hard to identify. In the present-day record there is not yet clear evidence for sustained changes in the CO_2 burden that directly relate to climate change feedbacks and which cannot be explained within the uncertainty of quantifying anthropogenic fossil fuel emissions and land use changes. In contrast, given methane's lifetime, it can serve as a "tallying-together" of ongoing climate change impacts, a representative bellwether.

Methane is a good integrative signal of the state of global wetlands, and methane's global budget—its growth or decline when the burden in the air is not in equilibrium with the net flux from sources and sinks—sums the changing breath of the whole land biosphere. This includes not only changing outputs from biogenic sources (nearly all terrestrial or coastal, not oceanic) such as tropical and boreal wetlands, grass and tree growth for ruminants, and growth in biomass fire fuel loads, but also changes in the meteorologically sensitive oxidative capacity of the atmosphere involving [OH] Cl, and soil uptake. All natural sources and sinks are highly variable with climate fluctuation. Wetland and ruminant emissions vary with plant growth, rapidly changing as precipitation and temperature shift in ENSO and IOD cycles, and as CO_2 varies. Methane removal by [OH] (especially in the tropical mid-troposphere) and Cl fluctuates with the intensity of the Inter-Tropical Convergence and the trade winds in the ENSO cycles. Hydroxyl is also sensitive to atmospheric NO_x, for example from dry season tropical fires, since the paleolithic often human-lit. Soil sinks in aerated soils, capable of breathing as pressure fluctuates under frontal passage are climate-dependent, as bacterial methanotrophy needs the right conditions, neither too dry nor too wet.

If the climate is constant, then the methane burden equilibrates and is steady. When the climate changes, natural methane sources and sinks respond and there is consequent disequilibrium in the methane budget (i.e., growth or decline of the burden). Sustained disequilibrium in the methane burden thus signals ongoing change in the biological productivity of the entire planet's land surface. With the isotopic spin-up taking several decades, a long-sustained growth or decline indicates a multi-decade change that is outside decadal variability.

The abruptness, power and global scale of past glacial/interglacial terminations provide paleoclimatological standards for comparison with what is taking place today (Tzedakis et al., 2009). The Eemian interglacial (130–115 ka BP, Marine Isotopic Stage 5, initiated by Termination II) was warmest around 125,000 years ago, with sea level perhaps 6–9 m above present-day level, implying significant melting both in Greenland and Antarctica compared to today (Dutton & Lambeck, 2012). The Eemian "green Sahara" had abundant wetlands and great lakes (Larrasoana et al., 2013), very different from the current climate. However, the Eemian may be a poor guide to the future. Such past records may give little predictive help: the driving force today is anthropogenic, the speed of growth in CO_2 and CH_4 burdens is unprecedented, as is global land use change, so what is to come may be warmer than recent interglacials, even the Eemian.

The model growth curve in Figures 12a and 12b assumes growth that may be below what will occur in the next decade if both natural and anthropogenic emissions rise strongly. However, assuming the emission growth rates in the model, the increased radiative forcing of the climate from this extra methane input from the years 2021–2036 can be estimated at roughly 0.17 W/m^2. To put this in context, that is about equivalent to perhaps five years of ongoing growth in CO_2 forcing. There are important consequences for climate modelers. Using a methane-enabled Earth System Model, Kleinen et al. (2021) found methane mixing ratios and hence radiative forcing substantially higher than assumed in the scenarios used for the Coupled Model Intercomparison Project; assuming methane growth is only due to anthropogenic causes may lead to underestimation of future change.

The question remains open. The observed post-2006 CH_4 growth (Figure 1) is comparable to growth during the abrupt phase of a termination. Top-down and bottom-up estimates of modern emission growth rates are comparable to or greater than growth in termination events. Modeling shows that the modern record is comparable to termination events both for the change in CH_4 abundance driven by natural sources and that there are parallels between the observed modern $\delta^{13}C_{CH4}$ record and the isotopic records during full terminations.

Methane's unexpected rise means achieving the Paris Agreement's targets will be very difficult (Mikaloff-Fletcher & Schaefer, 2019; Nisbet et al., 2020) and will likely demand accelerated switching from fossil fuels to renewable energy sources, in addition to rapid elimination of methane emissions from fossil fuel use. Reducing the methane burden to its pre-industrial size would have beneficial impacts not only on climate, but also on air quality, increasing the oxidizing capacity of the atmosphere (Staniaszek et al., 2022). Shooting the methane messenger will not eliminate methane's message. But it would help.

A casual coincidence does not confirm a causal connection. That we are in the midst of an rapid methane growth event, substantially driven by natural sources, does not necessarily mean the onset of global climate change. There is still the possibility that we are simply experiencing decadal- or centennial-scale variability. But past decadal- and centennial- scale Holocene variability, while significant, is smaller and much less abrupt than the typical abrupt climate change. Moreover, rapid growth in natural methane emissions does not happen unless climate is changing also: thus methane may indeed be the bellwether, the first indicator, the messenger of climate change.

There are limits to comparison. Applying the designation "termination" to current changes is not strictly correct in the modern usage of Terminations IX to I. Yet Broecker and Denton (1990) originally recognized terminations in the wider sense as "massive and abrupt reorganizations of the ocean-atmosphere system." In this sense, such an event may already be taking place. The remarkable shifts in the biogenic methane budget since the end of 2006 may be a first indicator of a large-scale reorganization of the climate system on a scale that matches past great changes. Any current or near-future warming transition will differ greatly from the past glacial-interglacial Terminations IX to I. There is no Roman number zero. But then, zero is different from all other numbers. The question is valid: have we already entered Termination Zero?

Data Availability Statement

All data sources are public and listed in the figure captions. The main repositories are the data archives of US National Atmospheric and Oceanic Administration (https://gml.noaa.gov/aftp/data/trace_gases/ch4c13/flask/surface/) and NIWA and other data in the World Data Center for Greenhouse Gases https://gaw.kishou.go.jp/. Reference to the European Commission's EDGAR data sets is from The Global Greenhouse Emissions. Emissions Database for Global Atmospheric Research V7.0. https://edgar.jrc.ec.europa.eu/dataset_ghg70 , which was accessed at various dates up to 15/01/2023.

Acknowledgments
EGN, DL, REF, JLF, and the Royal Holloway laboratory thank the UK Met Office for three decades of support on Ascension Island. We thank NILU-Norway, IUP Heidelberg, and Environment Canada for sampling at Zeppelin, Svalbard and Alert, Canada, the South African Weather Service for sampling at Cape Point, and the British Antarctic Survey . D.Lowe and K.Lassey of NIWA New Zealand and I.Levin of IUP Heidelberg helped generously in our early start-up, as did P.Crutzen, R. Cicerone and A. Roddy. EGN thanks the UK Natural Environment Research Council for grants NE/S00159X/1 ZWAMPS Quantifying Methane Emissions in remote tropical settings: a new 3D approach and NE/N016238/1 MOYA: The Global Methane Budget, and colleagues involved with the UNEP International Methane Emissions Observatory for discussions and insight. XL thanks NOAA Cooperative agreement NA22OAR4320151. REF thanks NERC for Grant NE/V000780/1 Methane D/H Discovering reasons for global atmospheric methane growth using deuterium isotopes. PIP acknowledges support from the UK National Centre for Earth Observation funded by the Natural Environment Research Council (NE/R016518/1). TR's laboratory was supported in part by the European Union's Marie Curie project MEMO^2 (Methane goes Mobile—Measurements and Modeling) and ATMO ACCESS.

References

Abram, N. J., Hargreaves, J. A., Wright, N. M., Thirumalai, K., Ummenhofer, C. C., & England, M. H. (2020). Palaeoclimate perspectives on the Indian Ocean dipole. *Quaternary Science Reviews*, *237*, 106302. https://doi.org/10.1016/j.quascirev.2020.106302

Ackerman, D., Millet, D. B., & Chen, X. (2019). Global estimates of inorganic nitrogen deposition across four decades. *Global Biogeochemical Cycles*, *33*(1), 100–107. https://doi.org/10.1029/2018gb005990

Barker, P. A., Allen, G., Gallagher, M., Pitt, J. R., Fisher, R. E., Bannan, T., et al. (2020). Airborne measurements of fire emission factors for African biomass burning sampled during the MOYA campaign. *Atmospheric Chemistry and Physics*, *20*(23), 15443–15459. https://doi.org/10.5194/acp-20-15443-2020

Basu, S., Lan, X., Dlugokencky, E., Michel, S., Schwietzke, S., Miller, J. B., et al. (2022). Estimating emissions of methane consistent with atmospheric measurements of methane and $\delta^{13}C$ of methane. *Atmospheric Chemistry and Physics*, *22*(23), 15351–15377. https://doi.org/10.5194/acp-22-15351-2022

Baumgartner, M., Schilt, A., Eicher, O., Schmitt, J., Schwander, J., Spahni, R., et al. (2012). High-resolution interpolar difference of atmospheric methane around the Last Glacial Maximum. *Biogeosciences*, *9*, 3961–3977. https://doi.org/10.5194/bg-9-3961-2012

Bereiter, B., Eggleston, S., Schmitt, J., Nehrbass-Ahles, C., Stocker, T. F., Fischer, H., et al. (2015). Revision of the EPICA Dome C CO_2 record from 800 to 600 kyr before present. *Geophysical Research Letters*, *42*(2), 542–549. https://doi.org/10.1002/2014gl061957

Berner, L. T., Massey, R., Jantz, P., Forbes, B. C., Macias-Fauria, M., Myers-Smith, I., et al. (2020). Summer warming explains widespread but not uniform greening in the Arctic tundra biome. *Nature Communications*, *11*, 1–12. https://doi.org/10.1038/s41467-020-18479-5

Bock, M., Schmitt, J., Beck, J., Seth, B., Chappellaz, J., & Fischer, H. (2017). Glacial/interglacial wetland, biomass burning, and geologic methane emissions constrained by dual stable isotopic CH_4 ice core records. *Proceedings of the National Academy of Sciences of the United States of America*, *114*(29), E5778–E5786. https://doi.org/10.1073/pnas.1613883114

Boers, N., Ghil, M., & Rousseau, D. D. (2018). Ocean circulation, ice shelf, and sea ice interactions explain Dansgaard–Oeschger cycles. *Proceedings of the National Academy of Sciences*, *115*(47), E11005-14. https://doi.org/10.1073/pnas.1802573115

Bonnet, R., Swingedouw, D., Gastineau, G., Boucher, O., Deshayes, J., Hourdin, F., et al. (2021). Increased risk of near term global warming due to a recent AMOC weakening. *Nature Communications*, *12*(1), 1–9. https://doi.org/10.1038/s41467-021-26370-0

Brierley, C., Thirumalai, K., Grindrod, E., & Barnsley, J. (2023). Indian ocean variability changes in the paleoclimate modelling intercomparison project. *Climate of the Past*, *19*(3), 681–701. https://doi.org/10.5194/cp-19-681-2023

Broecker, W. S., & Denton, G. H. (1990). The role of ocean-atmosphere reorganizations in glacial cycles. *Quaternary Science Reviews*, *9*(4), 305–341. https://doi.org/10.1016/0277-3791(90)90026-7

Broecker, W. S., & Van Donk, J. (1970). Insolation changes, ice volumes, and the O18 record in deep-sea cores. *Reviews of Geophysics*, *8*(1), 169–198. https://doi.org/10.1029/rg008i001p00169

Brownlow, R., Lowry, D., Fisher, R. E., France, J. L., Lanoisellé, M., White, B., et al. (2017). Isotopic ratios of tropical methane emissions by atmospheric measurement. *Global Biogeochemical Cycles*, *31*(9), 1408–1419. https://doi.org/10.1002/2017gb005689

Cai, W., Wu, L., Lengaigne, M., Li, T., McGregor, S., Kug, J. S., et al. (2019). Pantropical climate interactions. *Science*, *363*(6430), eaav4236. https://doi.org/10.1126/science.aav4236

Cantrell, C. A., Shetter, R. E., McDaniel, A. H., Calvert, J. G., Davidson, J. A., Lowe, D. C., et al. (1990). Carbon kinetic isotope effect in the oxidation of methane by the hydroxyl radical. *Journal of Geophysical Research*, *95*(D13), 22455–22462. https://doi.org/10.1029/jd095id13p22455

Capron, E., Rasmussen, S. O., Popp, T. J., Erhardt, T., Fischer, H., Landais, A., et al. (2021). The anatomy of past abrupt warmings recorded in Greenland ice. *Nature Communications*, *12*(1), 2106. https://doi.org/10.1038/s41467-021-22241-w

Chang, J., Peng, S., Ciais, P., Saunois, M., Dangal, S. R. S., Herrero, M., et al. (2019). Revisiting enteric methane emissions from domestic ruminants and their $\delta^{13}C_{CH4}$ source signature. *Nature Communications*, *10*(1), 3420. https://doi.org/10.1038/s41467-019-11066-3

Chang, K. Y., Riley, W. J., Collier, N., McNicol, G., Fluet-Chouinard, E., Knox, S. H., et al. (2023). Observational constraints reduce model spread but not uncertainty in global wetland methane emission estimates. *Global Change Biology*, *29*(15), 4298–4312. https://doi.org/10.1111/gcb.16755

Cheng, H., Edwards, R. L., Broecker, W. S., Denton, G. H., Kong, X., Wang, Y., et al. (2009). Ice age terminations. *Science*, *326*(5950), 248–252. https://doi.org/10.1126/science.1177840

Cheng, H., Zhang, H., Spötl, C., Baker, J., Sinha, A., Li, H., et al. (2020). Timing and structure of the Younger Dryas event and its underlying climate dynamics. *Proceedings of the National Academy of Sciences*, *117*(38), 23408–23417. https://doi.org/10.1073/pnas.2007869117
Cheng, L. J., Abraham, J., Trenberth, K. E., Fasullo, J., Boyer, T., Mann, M. E., et al. (2023). Another year of record heat for the oceans. *Advances in Atmospheric Sciences*, *40*(6), 963–974. https://doi.org/10.1007/s00376-023-2385-2
Cheng, W., Bitz, C. M., & Chiang, J. C. (2007). Adjustment of the global climate to an abrupt slowdown of the Atlantic meridional overturning circulation. *Geophysical Monograph-American Geophysical Union*, *173*, 295. https://doi.org/10.1029/173GM19
Clauss, M., Dittmann, M. T., Vendl, C., Hagen, K. B., Frei, S., Ortmann, S., et al. (2020). Comparative methane production in mammalian herbivores. *Animal*, *14*, s113–s123. https://doi.org/10.1017/s1751731119003161
Cleveland, R. B., Cleveland, W. S., McRae, J. E., & Terpenning, I. (1990). STL: A seasonal-trend decomposition. *Journal of Official Statistics*, *6*, 3–73.
Cooper, M. J., Martin, R. V., Hammer, M. S., Levelt, P. F., Veefkind, P., Lamsal, L. N., et al. (2022). Global fine-scale changes in ambient NO_2 during COVID-19 lockdowns. *Nature*, *601*(7893), 380–387. https://doi.org/10.1038/s41586-021-04229-0
Craig, H., Chou, C. C., Welhan, J. A., Stevens, C. M., & Engelkemeir, A. (1988). The isotopic composition of methane in polar ice cores. *Science*, *242*(4885), 1535–1539. https://doi.org/10.1126/science.242.4885.1535
Crippa, M., Guizzardi, D., Solazzo, E., Muntean, M., Schaaf, E., Monforti-Ferrario, F., et al. (2021). *GHG emissions of all world countries—2021 Report, EUR 30831 EN*. Publications Office of the European Union. https://doi.org/10.2760/173513
Curry, C. L. (2007). Modeling the soil consumption of atmospheric methane at the global scale. *Global Biogeochemical Cycles*, *21*(4), GB4012. https://doi.org/10.1029/2006GB002818
Dangal, S. R., Tian, H., Xu, R., Chang, J., Canadell, J. G., Ciais, P., et al. (2019). Global nitrous oxide emissions from pasturelands and rangelands: Magnitude, spatiotemporal patterns, and attribution. *Global Biogeochemical Cycles*, *33*(2), 200–222. https://doi.org/10.1029/2018gb006091
Dean, J. F., Middelburg, J. J., Röckmann, T., Aerts, R., Blauw, L. G., Egger, M., et al. (2018). Methane feedbacks to the global climate system in a warmer world. *Reviews of Geophysics*, *56*(1), 207–250. https://doi.org/10.1002/2017rg000559
Denton, G. H., Anderson, R. F., Toggweiler, J. R., Edwards, R. L., Schaefer, J. M., & Putnam, A. E. (2010). The last glacial termination. *Science*, *328*(5986), 1652–1656. https://doi.org/10.1126/science.1184119
Ditlevsen, P., & Ditlevsen, S. (2023). Warning of a forthcoming collapse of the Atlantic meridional overturning circulation. *Nature Communications*, *14*, 4254. https://doi.org/10.1038/s41467-023-39810-w
Dlugokencky, E. J., Houweling, S., Bruhwiler, L., Masarie, K. A., Lang, P. M., Miller, J. B., & Tans, P. P. (2003). Atmospheric methane levels off: Temporary pause or a new steady-state? *Geophysical Research Letters*, *30*(19), 1992. https://doi.org/10.1029/2003gl018126
Dlugokencky, E. J., Masarie, K. A., Lang, P. M., & Tans, P. P. (1998). Continuing decline in the growth rate of the atmospheric methane burden. *Nature*, *393*(6684), 447–450. https://doi.org/10.1038/30934
Dlugokencky, E. J., Masaire, K. A., Lang, P. M., Tans, P. P., Steele, L. P., & Nisbet, E. G. (1994). A dramatic decrease in the growth rate of atmospheric methane in the northern hemisphere during 1992. *Geophysical Research Letters*, *21*(1), 45–48. https://doi.org/10.1029/93gl03070
Dlugokencky, E. J., Nisbet, E. G., Fisher, R., & Lowry, D. (2011). Global atmospheric methane: Budget, changes and dangers. *Philosophical Transactions of the Royal Society A: Mathematical, Physical & Engineering Sciences*, *369*(1943), 2058–2072. https://doi.org/10.1098/rsta.2010.0341
Drinkwater, A., Palmer, P., Feng, L., Arnold, T., Lan, X., Michel, S., et al. (2022). Atmospheric data support a multi-decadal shift in the global methane budget towards natural tropical emissions. In *Atmospheric chemistry and physics discussions* (pp. 1–35).
Dutton, A., & Lambeck, K. (2012). Ice volume and sea level during the last interglacial. *Science*, *337*(6091), 216–219. https://doi.org/10.1126/science.1205749
Dutton, C. L., Subalusky, A. L., Sanchez, A., Estrela, S., Lu, N., Hamilton, S. K., et al. (2021). The meta-gut: community coalescence of animal gut and environmental microbiomes. *Scientific Reports*, *11*(1). https://doi.org/10.1038/s41598-021-02349-1
EDGAR. (2023). Global Greenhouse emissions. Emissions database for global atmospheric Research V7.0. Retrieved from https://edgar.jrc.ec.europa.eu/dataset_ghg70
Ehhalt, D. H. (1974). The atmospheric cycle of methane. *Tellus*, *26*(1–2), 58–70. https://doi.org/10.3402/tellusa.v26i1-2.9737
Erhardt, T., Capron, E., Rasmussen, S. O., Schüpbach, S., Bigler, M., Adolphi, F., & Fischer, H. (2019). Decadal-scale progression of the onset of Dansgaard–Oeschger warming events. *Climate of the Past*, *15*, 811–825. https://doi.org/10.5194/cp-15-811-2019
Etheridge, D. M., Steele, L., Francey, R. J., & Langenfelds, R. L. (1998). Atmospheric methane between 1000 AD and present: Evidence of anthropogenic emissions and climatic variability. *Journal of Geophysical Research*, *103*(D13), 15979-93–15993. https://doi.org/10.1029/98jd00923
FAO. (2017). World fertilizer trends and outlook to 2020. Retrieved from https://www.fao.org/3/i6895e/i6895e.pdf
Feng, L., Palmer, P. I., Parker, R. J., Lunt, M. F., & Bösch, H. (2023). Methane emissions are predominantly responsible for record-breaking atmospheric methane growth rates in 2020 and 2021. *Atmospheric Chemistry and Physics*, *23*(8), 4863–4880. https://doi.org/10.5194/acp-23-4863-2023
Feng, L., Palmer, P. I., Zhu, S., Parker, R. J., & Liu, Y. (2022). Tropical methane emissions explain large fraction of recent changes in global atmospheric methane growth rate. *Nature Communications*, *13*, 1–8. https://doi.org/10.1038/s41467-022-28989-z
Ferretti, D. F., Miller, J. B., White, J. W., Etheridge, D. M., Lassey, K. R., Lowe, D. C., et al. (2005). Unexpected changes to the global methane budget over the past 2000 years. *Science*, *309*(5741), 1714-7–1717. https://doi.org/10.1126/science.1115193
Fischer, H., Behrens, M., Bock, M., Richter, U., Schmitt, J., Loulergue, L., et al. (2008). Changing boreal methane sources and constant biomass burning during the last termination. *Nature*, *452*(7189), 864–867. https://doi.org/10.1038/nature06825
Fowler, D., Coyle, M., Skiba, U., Sutton, M. A., Cape, J. N., Reis, S., et al. (2013). The global nitrogen cycle in the twenty-first century. *Philosophical Transactions of the Royal Society B: Biological Sciences*, *368*(1621), 20130164. https://doi.org/10.1098/rstb.2013.0164
France, J. L., Fisher, R. E., Lowry, D., Lanoiselle, M., Nisbet-Jones, P. B. R., Andrade, M., et al. (2021). $\delta^{13}C$ methane source signatures from tropical wetland and rice field emissions. *Philosophical Transactions of the Royal Society A*, *380*(2215), 20200449. https://doi.org/10.1098/rsta.2020.0449
France, J. L., Lunt, M. F., Andrade, M., Moreno, I., Ganesan, A. L., Lachlan-Cope, T., et al. (2022). Very large fluxes of methane measured above Bolivian seasonal wetlands. *Proceedings of the National Academy of Sciences*, *119*(32), e2206345119. https://doi.org/10.1073/pnas.2206345119
Ganesan, A. L., Stell, A. C., Gedney, N., Comyn-Platt, E., Hayman, G., Rigby, M., et al. (2018). Spatially resolved isotopic source signatures of wetland methane emissions. *Geophysical Research Letters*, *45*(8), 3737–3745. https://doi.org/10.1002/2018gl077536
Gauci, V., Fowler, D., Chapman, S. J., & Dise, N. B. (2005). Sulfate deposition and temperature controls on methane emission and sulfur forms in peat. *Biogeochemistry*, *71*(2), 141–162. https://doi.org/10.1007/s10533-005-0681-9
Geng, T., Cai, W., Wu, L., Santoso, A., Wang, G., Jing, Z., et al. (2022). Emergence of changing central-Pacific and eastern-Pacific El Niño-southern oscillation in a warming climate. *Nature Communications*, *13*, 1–11. https://doi.org/10.1038/s41467-022-33930-5

Gloor, M., Gatti, L. V., Wilson, C., Parker, R. J., Boesch, H., Popa, E., et al. (2021). Large methane emissions from the Pantanal during rising water-levels revealed by regularly measured lower troposphere CH_4 profiles. *Global Biogeochemical Cycles*, *35*(10), e2021GB006964. https://doi.org/10.1029/2021GB006964

Gorbatenko, V. P., Pustovalov, K. N., & Konstantinova, D. A. (2020). Convective potential of the atmosphere of Western Siberia amid global climate change. In *IOP conference series: Earth and environmental science*. (Vol. 611, p. 012001). IOP Publishing.

Graven, H. D., Keeling, R. F., Piper, S. C., Patra, P. K., Stephens, B. B., Wofsy, S. C., et al. (2013). Enhanced seasonal exchange of CO_2 by northern ecosystems since 1960. *Science*, *341*(6150), 1085–1089. https://doi.org/10.1126/science.1239207

Grise, K. M., Davis, S. M., Simpson, I. R., Waugh, D. W., Fu, Q., Allen, R. J., et al. (2019). Recent tropical expansion: Natural variability or forced response? *Journal of Climate*, *32*(5), 1551–1571. https://doi.org/10.1175/jcli-d-18-0444.1

Hasan, N. A., Chikamoto, Y., & McPhaden, M. J. (2022). The influence of tropical basin interactions on the 2020–2022 double-dip La Niña. *Frontiers in Climate*, *4*, 1001174. https://doi.org/10.3389/fclim.2022.1001174

Haverd, V., Smith, B., Canadell, J. G., Cuntz, M., Mikaloff-Fletcher, S., Farquhar, G., et al. (2020). Higher than expected CO_2 fertilization inferred from leaf to global observations. *Global Change Biology*, *26*(4), 2390–2402. https://doi.org/10.1111/gcb.14950

Holden, P. B., Edwards, N. R., Gerten, D., & Schaphoff, S. (2013). A model-based constraint on CO_2 fertilisation. *Biogeosciences*, *10*(1), 339–355. https://doi.org/10.5194/bg-10-339-2013

Hossaini, R., Chipperfield, M. P., Saiz-Lopez, A., Fernandez, R., Monks, S., Feng, W., et al. (2016). A global model of tropospheric chlorine chemistry: Organic versus inorganic sources and impact on methane oxidation. *Journal of Geophysical Research: Atmospheres*, *121*(23), 14271–14297. https://doi.org/10.1002/2016JD025756

Howarth, R. W. (2019). Ideas and perspectives: Is shale gas a major driver of recent increase in global atmospheric methane? *Biogeosciences*, *16*(15), 3033–3046. https://doi.org/10.5194/bg-16-3033-2019

Huntingford, C., Burke, E. J., Jones, C. D., Jeffers, E. S., & Wiltshire, A. J. (2022). Nitrogen cycle impacts on CO_2 fertilisation and climate forcing of land carbon stores. *Environmental Research Letters*, *17*(4), 044072. https://doi.org/10.1088/1748-9326/ac6148

IEA. (2022). Global methane emissions from the energy sector over time, 2000-2021. Retrieved from https://www.iea.org/data-and-statistics/charts/global-methane-emissions-from-the-energy-sector-over-time-2000-2021

IFAstat. (2022). International fertilizer association database 1.1. Fertilizer consumption—Historical trends by country or region. Retrieved from https://www.ifastat.org/databases/graph/1_1

IPCC. (2021). Figure 8.11, chapter 8. In *Climate change 2021: The physical science basis. Contribution of working group I to the sixth assessment report of the intergovernmental panel on climate change* (pp. 1055–1210). Cambridge University Press. https://doi.org/10.1017/9781009157896.010

Jo, H.-S., Ham, Y.-G., Kug, J.-S., Li, T., Kim, J.-H., Kim, J.-G., & Kim, H. (2022). Southern Indian Ocean Dipole as a trigger for central Pacific El Niño since the 2000s. *Nature Communications*, *13*(1), 6965. https://doi.org/10.1038/s41467-022-34721-8

Kim, Y. H., Min, S. K., Gillett, N. P., Notz, D., & Malinina, E. (2023). Observationally-constrained projections of an ice-free Arctic even under a low emission scenario. *Nature Communications*, *14*(1), 3139. https://doi.org/10.1038/s41467-023-38511-8

Kleinen, T., Gromov, S., Steil, B., & Brovkin, V. (2021). Atmospheric methane underestimated in future climate projections. *Environmental Research Letters*, *16*(9), 094006. https://doi.org/10.1088/1748-9326/ac1814

Lan, X., Basu, S., Schwietzke, S., Bruhwiler, L. M., Dlugokencky, E. J., Michel, S. E., et al. (2021). Improved constraints on global methane emissions and sinks using $\delta^{13}C$-CH_4. *Global Biogeochemical Cycles*, *35*(6), e2021GB007000. https://doi.org/10.1029/2021gb007000

Lan, X., Dlugokencky, E. J., Mund, J. W., Crotwell, A. M., Crotwell, M. J., Moglia, E., et al. (2022). Atmospheric methane dry air mole fractions from the NOAA GML carbon cycle cooperative global air sampling network, 1983–2021, version: 2022-11-21. https://doi.org/10.15138/VNCZ-M766

Lan, X., Nisbet, E. G., Dlugokencky, E. J., & Michel, S. E. (2021). What do we know about the global methane budget? Results from four decades of atmospheric CH_4 observations and the way forward. *Philosophical Transactions of the Royal Society A*, *379*(2210), 20200440. https://doi.org/10.1098/rsta.2020.0440

Lan, X., Thoning, K. W., & Dlugokencky, E. J. (2023). Trends in globally-averaged CH_4, N_2O, and SF6 determined from NOAA global monitoring laboratory measurements. Version 2022-11. https://doi.org/10.15138/P8XG-AA10. Retrieved from https://gml.noaa.gov/webdata/ccgg/trends/ch4/ch4_annmean_gl.txt

Lang, N., & Wolff, E. W. (2011). Interglacial and glacial variability from the last 800 ka in marine, ice and terrestrial archives. *Climate of the Past*, *7*(2), 361–380. https://doi.org/10.5194/cp-7-361-2011

Larrasoana, J. C., Roberts, A. P., & Rohling, E. J. (2013). Dynamics of green Sahara periods and their role in Hominin evolution. *PLoS One*, *8*(10), e76514. https://doi.org/10.1371/journal.pone.0076514

Lassey, K. R., Lowe, D. C., & Smith, A. M. (2007). The atmospheric cycling of radiomethane and the "fossil fraction" of the methane source. *Atmospheric Chemistry and Physics*, *7*(8), 2141–2149. https://doi.org/10.5194/acp-7-2141-2007

Laughner, J. L., Neu, J. L., Schimel, D., Wennberg, P. O., Barsanti, K., Bowman, K. W., et al. (2021). Societal shifts due to COVID-19 reveal large-scale complexities and feedbacks between atmospheric chemistry and climate change. *Proceedings of the National Academy of Sciences*, *118*(46), e2109481118. https://doi.org/10.1073/pnas.2109481118

Leitner, S., Carbonell, V., Butterbach-Bahl, K., Barthel, M., Mhindu, R. L., Mutuo, P., et al. (2023). Traditional livestock enclosures are greenhouse gas hotspots in the African savanna landscape: The case of a rangeland in Kenya. In *EGU general assembly 2023, Vienna, Austria, 24–28 Apr 2023, EGU23-14773*. https://doi.org/10.5194/egusphere-egu23-14773

Levin, I., Veidt, C., Vaughn, B. H., Brailsford, G., Bromley, T., Heinz, R., et al. (2012). No inter-hemispheric $\delta^{13}CH_4$ trend observed. *Nature*, *486*(7404), E3–E4. https://doi.org/10.1038/nature11175

Liu, J., Wu, D., Xu, X., Ji, M., Chen, Q., & Wang, X. (2021). Projection of extreme precipitation induced by Arctic amplification over the Northern Hemisphere. *Environmental Research Letters*, *16*(7), 074012. https://doi.org/10.1088/1748-9326/ac0acc

Lobell, D. B., & Field, C. B. (2008). Estimation of the carbon dioxide (CO_2) fertilization effect using growth rate anomalies of CO_2 and crop yields since 1961. *Global Change Biology*, *14*(1), 39–45. https://doi.org/10.1111/j.1365-2486.2007.01476.x

Loulergue, L., Schilt, A., Spahni, R., Masson-Delmotte, V., Blunier, T., Lemieux, B., et al. (2008). Orbital and millennial-scale features of atmospheric CH_4 over the past 800,000 years. *Nature*, *453*(7193), 383–386. https://doi.org/10.1038/nature06950

Lowe, D. C., Brenninkmeijer, C. A., Brailsford, G. W., Lassey, K. R., Gomez, A. J., & Nisbet, E. G. (1994). Concentration and ^{13}C records of atmospheric methane in New Zealand and Antarctica: Evidence for changes in methane sources. *Journal of Geophysical Research*, *99*(D8), 16913–16925. https://doi.org/10.1029/94jd00908

Lowe, D. C., Brenninkmeijer, C. A., Manning, M. R., Sparks, R., & Wallace, G. (1988). Radiocarbon determination of atmospheric methane at Baring Head, New Zealand. *Nature*, *332*(6164), 522–525. https://doi.org/10.1038/332522a0

Lowe, D. C., Brenninkmeijer, C. A., Tyler, S. C., & Dlugokencky, E. J. (1991). Determination of the isotopic composition of atmospheric methane and its application in the Antarctic. *Journal of Geophysical Research*, *96*(D8), 15455–15467. https://doi.org/10.1029/91jd01119

Ludemann, C. I., Gruere, A., Heffer, P., & Dobermann, A. (2022). Global data on fertilizer use by crop and by country. *Scientific Data*, *9*, 1–8. https://doi.org/10.1038/s41597-022-01592-z

Lunt, M. F., Palmer, P. I., Feng, L., Taylor, C. M., Boesch, H., & Parker, R. J. (2019). An increase in methane emissions from tropical Africa between 2010 and 2016 inferred from satellite data. *Atmospheric Chemistry and Physics*, *19*(23), 14721–14740. https://doi.org/10.5194/acp-19-14721-2019

Lunt, M. F., Palmer, P. I., Lorente, A., Borsdorff, T., Landgraf, J., Parker, R. J., & Boesch, H. (2021). Rain-fed pulses of methane from East Africa during 2018–2019 contributed to atmospheric growth rate. *Environmental Research Letters*, *16*(2), 024021. https://doi.org/10.1088/1748-9326/abd8fa

Łupikasza, E. B., & Cielecka-Nowak, K. (2020). Changing probabilities of days with snow and rain in the Atlantic sector of the Arctic under the current warming trend. *Journal of Climate*, *33*(7), 2509–2532. https://doi.org/10.1175/jcli-d-19-0384.1

Matsumoto, K. (2007). Radiocarbon-based circulation age of the world oceans. *Journal of Geophysical Research*, *112*(C9), C09004. https://doi.org/10.1029/2007jc004095

Matthews, H. D. (2007). Implications of CO_2 fertilization for future climate change in a coupled climate–carbon model. *Global Change Biology*, *13*(5), 1068–1078. https://doi.org/10.1111/j.1365-2486.2007.01343.x

McPhaden, M. J., Hasan, N., & Chikamoto, Y. (2023). Causes and consequences of the prolonged 2020–2023 La Niña. In *EGU general assembly 2023, Vienna, Austria, 24–28 Apr 2023, EGU23-10801*. https://doi.org/10.5194/egusphere-egu23-10801

Melton, J. R., Schaefer, H., & Whiticar, M. J. (2012). Enrichment in ^{13}C of atmospheric CH_4 during the younger Dryas termination. *Climate of the Past*, *8*(4), 1177–1197. https://doi.org/10.5194/cp-8-1177-2012

Menoud, M., Van Der Veen, C., Lowry, D., Fernandez, J. M., Bakkaloglu, S., France, J. L., et al. (2022). New contributions of measurements in Europe to the global inventory of the stable isotopic composition of methane. *Earth System Science Data*, *14*(9), 4365–4386. https://doi.org/10.5194/essd-14-4365-2022

Michel, S. E., Clark, J. R., Vaughn, B. H., Crotwell, M., Madronich, M., Moglia, E., et al. (2022). *Stable isotopic composition of atmospheric methane (^{13}C) from the NOAA GML carbon cycle cooperative global air sampling network, 1998–2021. Version: 2022-12-15*. University of Colorado, Institute of Arctic and Alpine Research (INSTAAR). https://doi.org/10.15138/9p89-1x02

Mikaloff-Fletcher, S. E., & Schaefer, H. (2019). Rising methane: A new climate challenge. *Science*, *364*(6444), 932–933. https://doi.org/10.1126/science.aax1828

Milkov, A. V., Schwietzke, S., Allen, G., Sherwood, O. A., & Etiope, G. (2020). Using global isotopic data to constrain the role of shale gas production in recent increases in atmospheric methane. *Scientific Reports*, *10*(1), 4199. https://doi.org/10.1038/s41598-020-61035-w

Mischler, J. A., Sowers, T. A., Alley, R. B., Battle, M., McConnell, J. R., Mitchell, L., et al. (2009). Carbon and hydrogen isotopic composition of methane over the last 1000 years. *Global Biogeochemical Cycles*, *23*(4), GB4024. https://doi.org/10.1029/2009gb003460

Möller, L., Sowers, T., Bock, M., Spahni, R., Behrens, M., Schmitt, J., et al. (2013). Independent variations of CH_4 emissions and isotopic composition over the past 160,000 years. *Nature Geoscience*, *6*(10), 885–890. https://doi.org/10.1038/ngeo1922

Moseley, G. E., Spötl, C., Cheng, H., Boch, R., Min, A., & Edwards, R. L. (2015). Termination-II interstadial/stadial climate change recorded in two stalagmites from the north European Alps. *Quaternary Science Reviews*, *127*, 229–239. https://doi.org/10.1016/j.quascirev.2015.07.012

MOYA/ZWAMPS Team, Nisbet, E. G., Allen, G., Fisher, R. E., France, J. L., Lee, J. D., et al. (2021). Isotopic signatures of methane emissions from tropical fires, agriculture and wetlands: The MOYA and ZWAMPS flights. *Philosophical Transactions of the Royal Society A*, *380*(2215), 20210112. https://doi.org/10.1098/rsta.2021.0112

Myhre, G., Shindell, D., Bréon, F. M., Collins, W., Fuglestvedt, J., Huang, J., et al. (2013). Climate change 2013: The physical science basis. Contribution of working group I to the fifth assessment report of the intergovernmental panel on climate change. In *Anthropogenic and natural radiative forcing*. Cambridge University Press.

Nicely, J. M., Canty, T. P., Manyin, M., Oman, L. D., Salawitch, R. J., Steenrod, S. D., et al. (2018). Changes in global tropospheric OH expected as a result of climate change over the last several decades. *Journal of Geophysical Research: Atmospheres*, *123*(18), 10774–10795. https://doi.org/10.1029/2018JD028388

Nicholson, S. E. (2015). Long-term variability of the East African 'short rains' and its links to large-scale factors. *International Journal of Climatology*, *35*(13), 3979–3990. https://doi.org/10.1002/joc.4259

Nicholson, S. E., Fink, A. H., Funk, C., Klotter, D. A., & Satheesh, A. R. (2022). Meteorological causes of the catastrophic rains of October/November 2019 in equatorial Africa. *Global and Planetary Change*, *208*, 103687. https://doi.org/10.1016/j.gloplacha.2021.103687

Nisbet, E. G. (1990). The end of the ice age. *Canadian Journal of Earth Sciences*, *27*(1), 148–157. https://doi.org/10.1139/e90-012

Nisbet, E. G. (2022). Methane's unknowns better known. *Nature Geoscience*, *15*(11), 861–862. https://doi.org/10.1038/s41561-022-01049-3

Nisbet, E. G. (2023). Climate change feedback on methane emissions from global wetlands. *Nature Climate Change*, *13*(5), 421–422. https://doi.org/10.1038/s41558-023-01634-3

Nisbet, E. G., & Chappellaz, J. (2009). Shifting gear, quickly. *Science*, *324*(5926), 477–478. https://doi.org/10.1126/science.1172001

Nisbet, E. G., Dlugokencky, E. J., & Bousquet, P. (2014). Methane on the rise—Again. *Science*, *343*(6170), 493–495. https://doi.org/10.1126/science.1247828

Nisbet, E. G., Dlugokencky, E. J., Fisher, R. E., France, J. L., Lowry, D., Manning, M. R., et al. (2021). Atmospheric methane and nitrous oxide: Challenges along the path to Net Zero. *Philosophical Transactions of the Royal Society A*, *379*(2210), 20200457. https://doi.org/10.1098/rsta.2020.0457

Nisbet, E. G., Dlugokencky, E. J., Manning, M. R., Lowry, D., Fisher, R. E., France, J. L., et al. (2016). Rising atmospheric methane: 2007–2014 growth and isotopic shift. *Global Biogeochemical Cycles*, *30*(9), 1356–1370. https://doi.org/10.1002/2016gb005406

Nisbet, E. G., Fisher, R. E., Lowry, D., France, J. L., Allen, G., Bakkaloglu, S., et al. (2020). Methane mitigation: Methods to reduce emissions, on the path to the Paris agreement. *Reviews of Geophysics*, *58*(1), e2019RG000675. https://doi.org/10.1029/2019rg000675

Nisbet, E. G., Manning, M. R., Dlugokencky, E. J., Fisher, R. E., Lowry, D., Michel, S. E., et al. (2019). Very strong atmospheric methane growth in the 4 years 2014–2017: Implications for the Paris Agreement. *Global Biogeochemical Cycles*, *33*(3), 318–342. https://doi.org/10.1029/2018gb006009

NOAA. (2023a). CH4_annmean_gl.txt. Retrieved from https://gml.noaa.gov/webdata/ccgg/trends/ch4/ch4_annmean_gl.txt

NOAA. (2023b). SIO data. Retrieved from https://www.cpc.ncep.noaa.gov/data/indices/soi

Oh, Y., Zhuang, Q., Welp, L. R., Liu, L., Lan, X., Basu, S., et al. (2022). Improved global wetland carbon isotopic signatures support post-2006 microbial methane emission increase. *Communications Earth & Environment*, *3*(159), 1–12. https://doi.org/10.1038/s43247-022-00488-5

Osland, M. J., Stevens, P. W., Lamont, M. M., Brusca, R. C., Hart, K. M., Waddle, J. H., et al. (2021). Tropicalization of temperate ecosystems in North America: The northward range expansion of tropical organisms in response to warming winter temperatures. *Global Change Biology*, *27*(13), 3009–3034. https://doi.org/10.1111/gcb.15563

Palmer, P. I., Wainwright, C. M., Dong, B., Maidment, R. I., Wheeler, K. G., Gedney, N., et al. (2023). Drivers and impacts of Eastern African rainfall variability. *Nature Reviews Earth & Environment*, *4*, 254–270. https://doi.org/10.1038/s43017-023-00397-x

Pandey, S., Houweling, S., Krol, M., Aben, I., Monteil, G., Nechita-Banda, N., et al. (2017). Enhanced methane emissions from tropical wetlands during the 2011 La Niña. *Scientific Reports*, *7*, 1–8. https://doi.org/10.1038/srep45759

Pandey, S., Houweling, S., Krol, M., Aben, I., Nechita-Banda, N., Thoning, K., et al. (2019). Influence of atmospheric transport on estimates of variability in the global methane burden. *Geophysical Research Letters*, *46*(4), 2302–2311. https://doi.org/10.1029/2018gl081092

Peng, S., Lin, X., Thompson, R. L., Xi, Y., Liu, G., Hauglustaine, D., et al. (2022). Wetland emission and atmospheric sink changes explain methane growth in 2020. *Nature*, *612*(7940), 477–482. https://doi.org/10.1038/s41586-022-05447-w

Petrenko, V. V., Smith, A. M., Severinghaus, J. P., Brook, E. J., Lowe, D., Riedel, K., et al. (2009). $^{14}CH_4$ measurements in Greenland ice: Investigating last glacial termination CH_4 sources. *Science*, *324*, 506–508. https://doi.org/10.1126/science.1168909

Prather, M. J., Holmes, C. D., & Hsu, J. (2012). Reactive greenhouse gas scenarios: Systematic exploration of uncertainties and the role of atmospheric chemistry. *Geophysical Research Letters*, *39*(9), L09803. https://doi.org/10.1029/2012gl051440

Previdi, M., Smith, K. L., & Polvani, L. M. (2021). Arctic amplification of climate change: A review of underlying mechanisms. *Environmental Research Letters*, *16*(9), 093003. https://doi.org/10.1088/1748-9326/ac1c29

Qu, Z., Jacob, D. J., Zhang, Y., Shen, L., Varon, D. J., Lu, X., et al. (2022). Attribution of the 2020 surge in atmospheric methane by inverse analysis of GOSAT observations. *Environmental Research Letters*, *17*(9), 094003. https://doi.org/10.1088/1748-9326/ac8754

Quay, P. D., King, S. L., Lansdown, J. M., & Wilbur, D. O. (1988). Isotopic composition of methane released from wetlands: Implications for the increase in atmospheric methane. *Global Biogeochemical Cycles*, *2*(4), 385–397. https://doi.org/10.1029/gb002i004p00385

Quay, P. D., King, S. L., Stutsman, J., Wilbur, D. O., Steele, L. P., Fung, I., et al. (1991). Carbon isotopic composition of atmospheric CH_4: Fossil and biomass burning source strengths. *Global Biogeochemical Cycles*, *5*(1), 25–47. https://doi.org/10.1029/91gb00003

Raymo, M. E. (1997). The timing of major climate terminations. *Paleoceanography*, *12*(4), 577–585. https://doi.org/10.1029/97pa01169

Rhodes, R. H., Brook, E. J., Chiang, J. C., Blunier, T., Maselli, O. J., McConnell, J. R., et al. (2015). Enhanced tropical methane production in response to iceberg discharge in the North Atlantic. *Science*, *348*(6238), 1016–1019. https://doi.org/10.1126/science.1262005

Riddell-Young, B., Rosen, J., Brook, E., Buizert, C., Martin, K., Lee, J., et al. (2023). Tropical sources dominated methane changes of the last glacial maximum and deglaciation. https://doi.org/10.21203/rs.3.rs-2522042/v1

Ringeval, B., Houweling, S., Van Bodegom, P. M., Spahni, R., Van Beek, R., Joos, F., & Röckmann, T. (2014). Methane emissions from floodplains in the Amazon Basin: Challenges in developing a process-based model for global applications. *Biogeosciences*, *11*(6), 1519–1558. https://doi.org/10.5194/bg-11-1519-2014

Riveiros, N. V., Waelbroeck, C., Skinner, L., Duplessy, J. C., McManus, J. F., Kandiano, E. S., & Bauch, H. A. (2013). The "MIS 11 paradox" and ocean circulation: Role of millennial scale events. *Earth and Planetary Science Letters*, *371*, 258–268. https://doi.org/10.1016/j.epsl.2013.03.036

Rosentreter, J. A., Borges, A. V., Deemer, B. R., Holgerson, M. A., Liu, S., Song, C., et al. (2021). Half of global methane emissions come from highly variable aquatic ecosystem sources. *Nature Geoscience*, *14*(4), 225–230. https://doi.org/10.1038/s41561-021-00715-2

Rubino, M., Etheridge, D. M., Thornton, D. P., Howden, R., Allison, C. E., Francey, R. J., et al. (2019). Revised records of atmospheric trace gases CO_2, CH_4, N_2O, and $\delta^{13}C$-CO_2 over the last 2000 years from Law Dome, Antarctica. *Earth System Science Data*, *11*(2), 473–492. https://doi.org/10.5194/essd-11-473-2019

Sapart, C. J., Monteil, G., Prokopiou, M., van de Wal, R. S., Kaplan, J. O., Sperlich, P., et al. (2012). Natural and anthropogenic variations in methane sources during the past two millennia. *Nature*, *490*(7418), 85–88. https://doi.org/10.1038/nature11461

Saunois, M., Stavert, A. R., Poulter, B., Bousquet, P., Canadell, J. G., Jackson, R. B., et al. (2020). The global methane budget 2000–2017. *Earth System Science Data*, *12*(3), 1561–1623. https://doi.org/10.5194/essd-12-1561-2020

Schaefer, H., Fletcher, S. E. M., Veidt, C., Lassey, K. R., Brailsford, G. W., Bromley, T. M., et al. (2016). A 21st-century shift from fossil-fuel to biogenic methane emissions indicated by $^{13}CH_4$. *Science*, *352*(6281), 80–84. https://doi.org/10.1126/science.aad2705

Schaefer, H., Whiticar, M. J., Brook, E. J., Petrenko, V. V., Ferretti, D. F., & Severinghaus, J. P. (2006). Ice record of $\delta^{13}C$ for atmospheric CH_4 across the Younger Dryas-Preboreal transition. *Science*, *313*(5790), 1109–1112. https://doi.org/10.1126/science.1126562

Schmitt, J., Schneider, R., Elsig, J., Leuenberger, D., Lourantou, A., Chappellaz, J., et al. (2012). Carbon isotope constraints on the deglacial CO_2 rise from ice cores. *Science*, *336*(6082), 711–714. https://doi.org/10.1126/science.1217161

Severinghaus, J. P., & Brook, E. J. (1999). Abrupt climate change at the end of the last glacial period inferred from trapped air in polar ice. *Science*, *286*(5441), 930–934. https://doi.org/10.1126/science.286.5441.930

Severinghaus, J. P., Sowers, T., Brook, E. J., Alley, R. B., & Bender, M. L. (1998). Timing of abrupt climate change at the end of the Younger Dryas interval from thermally fractionated gases in polar ice. *Nature*, *391*(6663), 141–146. https://doi.org/10.1038/34346

Sharmila, S., & Walsh, K. J. E. (2018). Recent poleward shift of tropical cyclone formation linked to Hadley cell expansion. *Nature Climate Change*, *8*(8), 730–736. https://doi.org/10.1038/s41558-018-0227-5

Shaw, J. T., Allen, G., Barker, P., Pitt, J. R., Pasternak, D., Bauguitte, S. J. B., et al. (2022). Large methane emission fluxes observed from tropical wetlands in Zambia. *Global Biogeochemical Cycles*, *36*(6), e2021GB007261. https://doi.org/10.1029/2021gb007261

Sherwood, O. A., Schwietzke, S., Arling, V. A., & Etiope, G. (2017). Global inventory of gas geochemistry data from fossil fuel, microbial and burning sources version 2021. *Earth System Science Data*, *9*(2), 639–656. https://doi.org/10.5194/essd-9-639-2017

Spahni, R., Chappellaz, J., Stocker, T. F., Loulergue, L., Hausammann, G., Kawamura, K., et al. (2005). Atmospheric methane and nitrous oxide of the late Pleistocene from Antarctic ice cores. *Science*, *310*(5752), 1317–1321. https://doi.org/10.1126/science.1120132

Spivakovsky, C. M., Logan, J. A., Montzka, S. A., Balkanski, Y. J., Foreman-Fowler, M., Jones, D. B. A., et al. (2000). Three dimensional climatological distribution of tropospheric OH: Update and evaluation. *Journal of Geophysical Research*, *105*(D7), 8931–8980. https://doi.org/10.1029/1999JD901006

Staniaszek, Z., Griffiths, P. T., Folberth, G. A., O'Connor Fiona, M., Luke, A. N., & Archibald, A. T. (2022). The role of future anthropogenic methane emissions in air quality and climate. *NPJ Climate and Atmospheric Science*, *5*(1), 21. https://doi.org/10.1038/s41612-022-00247-5

Staten, P. W., Grise, K. M., Davis, S. M., Karnauskas, K. B., Waugh, D. W., Maycock, A. C., et al. (2020). Tropical widening: From global variations to regional impacts. *Bulletin of the American Meteorological Society*, *101*(6), E897–E904. https://doi.org/10.1175/bams-d-19-0047.1

Steele, L. P., Dlugokencky, E. J., Lang, P. M., Tans, P. P., Martin, R. C., & Masarie, K. A. (1992). Slowing down of the global accumulation of atmospheric methane during the 1980s. *Nature*, *358*(6384), 313–316. https://doi.org/10.1038/358313a0

Stevenson, D. S., Derwent, R. G., Wild, O., & Collins, W. J. (2022). COVID-19 lockdown emission reductions have the potential to explain over half of the coincident increase in global atmospheric methane. *Atmospheric Chemistry and Physics*, *22*, 14243–14252. https://doi.org/10.5194/acp-22-14243-2022

Strode, S. A., Wang, J. S., Manyin, M., Duncan, B., Hossaini, R., Keller, C. A., et al. (2020). Strong sensitivity of the isotopic composition of methane to the plausible range of tropospheric chlorine. *Atmospheric Chemistry and Physics*, *20*(14), 8405-19–8419. https://doi.org/10.5194/acp-20-8405-2020

Studholme, J., Fedorov, A. V., Gulev, S. K., Emanuel, K., & Hodges, K. (2022). Poleward expansion of tropical cyclone latitudes in warming climates. *Nature Geoscience*, *15*(1), 14–28. https://doi.org/10.1038/s41561-021-00859-1

Sun, S., Fang, Y., Zu, Y., Liu, L., & Li, K. (2022). Increased occurrences of early Indian Ocean Dipole under global warming. *Science Advances*, *8*(47), eadd6025. https://doi.org/10.1126/sciadv.add6025

Tans, P. P. (1997). A note on isotopic ratios and the global atmospheric methane budget. *Global Biogeochemical Cycles*, *11*(1), 77–81. https://doi.org/10.1029/96gb03940

Taylor, R. D., & Walker, B. H. (1978). Comparisons of vegetation use and Herbivore biomass on a Rhodesian game and cattle ranch. *Journal of Applied Ecology*, *15*(2), 565–581. https://doi.org/10.2307/2402611

Thanwerdas, J., Saunois, M., Berchet, A., Pison, I., Vaughn, B. H., Michel, S. E., & Bousquet, P. (2022). Variational inverse modeling within the community inversion framework v1. 1 to assimilate $\delta^{13}C$ (CH_4) and CH_4: A case study with model LMDz-SACS. *Geoscientific Model Development*, *15*(12), 4831–4851. https://doi.org/10.5194/gmd-15-4831-2022

Thompson, R. L., Nisbet, E. G., Pisso, I., Stohl, A., Blake, D., Dlugokencky, E. J., et al. (2018). Variability in atmospheric methane from fossil fuel and microbial sources over the last three decades. *Geophysical Research Letters*, *45*(20), 11499–11508. https://doi.org/10.1029/2018GL078127

Tzedakis, P. C., Raynaud, D., McManus, J. F., Berger, A., Brovkin, V., & Kiefer, T. (2009). Interglacial diversity. *Nature Geoscience*, *2*(11), 751–755. https://doi.org/10.1038/ngeo660

Uddin, S., Löw, M., Parvin, S., Fitzgerald, G. J., Tausz-Posch, S., Armstrong, R., et al. (2018). Elevated CO_2 mitigates the effect of surface drought by stimulating root growth to access sub-soil water. *PLoS One*, *13*(6), e0198928. https://doi.org/10.1371/journal.pone.0198928

Umezawa, T., Brenninkmeijer, C. A., Röckmann, T., Van Der Veen, C., Tyler, S. C., Fujita, R., et al. (2018). Interlaboratory comparison of $\delta^{13}C$ and δD measurements of atmospheric CH_4 for combined use of data sets from different laboratories. *Atmospheric Measurement Techniques*, *11*(2), 1207–1231. https://doi.org/10.5194/amt-11-1207-2018

van Herpen, M. M. J. W., Li, Q., Saiz-Lopez, A., Liisberg, J. B., Röckmann, T., Cuevas, C. A., et al. (2023). Photocatalytic chlorine atom production on mineral dust–sea spray aerosols over the North Atlantic. *Proceedings of the National Academy of Sciences*, *120*(31). https://doi.org/10.1073/pnas.2303974120

Voigt, A., Albern, N., Ceppi, P., Grise, K., Li, Y., & Medeiros, B. (2021). Clouds, radiation, and atmospheric circulation in the present-day climate and under climate change. *Wiley Interdisciplinary Reviews: Climate Change*, *12*(2), e694. https://doi.org/10.1002/wcc.694

von Schuckmann, K., Minière, A., Gues, F., Cuesta-Valero, F. J., Kirchengast, G., Adusumilli, S., et al. (2023). Heat stored in the Earth system 1960–2020: Where does the energy go? *Earth System Science Data*, *15*(4), 1675–1709. https://doi.org/10.5194/essd-15-1675-2023

Wang, B., Luo, X., Yang, Y. M., Sun, W., Cane, M. A., Cai, W., et al. (2019). Historical change of El Niño properties sheds light on future changes of extreme El Niño. *Proceedings of the National Academy of Sciences*, *116*(45), 22512–22517. https://doi.org/10.1073/pnas.1911130116

Wang, P., Huang, Q., Liu, S., Cai, H., Yu, J., Wang, T., et al. (2022). Recent regional warming across the siberian lowlands: A comparison between permafrost and non-permafrost areas. *Environmental Research Letters*, *17*(5), 054047. https://doi.org/10.1088/1748-9326/ac6c9d

Wang, S., Zhang, Y., Ju, W., Chen, J. M., Ciais, P., Cescatti, A., et al. (2020). Recent global decline of CO_2 fertilization effects on vegetation photosynthesis. *Science*, *370*(6522), 1295–1300. https://doi.org/10.1126/science.abb7772

Wanner, H., Beer, J., Bütikofer, J., Crowley, T. J., Cubasch, U., Flückiger, J., et al. (2008). Mid-to late Holocene climate change: An overview. *Quaternary Science Reviews*, *27*(19–20), 1791–1828. https://doi.org/10.1016/j.quascirev.2008.06.013

Wen, X., Unger, V., Jurasinski, G., Koebsch, F., Horn, F., Rehder, G., et al. (2018). Predominance of methanogens over methanotrophs in rewetted fens characterized by high methane emissions. *Biogeosciences*, *15*(21), 6519–6536. https://doi.org/10.5194/bg-15-6519-2018

WMO. (2023). WMO global annual to decadal climate update (see appendix). Retrieved from https://hadleyserver.metoffice.gov.uk/wmolc/WMO_GADCU_2023-2027.pdf

Wolff, E. W., Chappellaz, J., Blunier, T., Rasmussen, S. O., & Svensson, A. (2010). Millennial-scale variability during the last glacial: The ice core record. *Quaternary Science Reviews*, *29*(21–22), 2828–2838. https://doi.org/10.1016/j.quascirev.2009.10.013

Wolff, E. W., Fischer, H., & Röthlisberger, R. (2009). Glacial terminations as southern warmings without northern control. *Nature Geoscience*, *2*(3), 206–209. https://doi.org/10.1038/ngeo442

Worden, J., Pandey, S., Zhang, Y., Cusworth, D., Zhen, Q., Bloom, A., et al. (2023). A bayesian framework for verifying methane inventories and trends with atmospheric methane data. In *EGU general assembly 2023, Vienna, Austria, 24–28 Apr 2023, EGU23-17172*. https://doi.org/10.5194/egusphere-egu23-17172

Worden, J. R., Bloom, A. A., Pandey, S., Jiang, Z., Worden, H. M., Walker, T. W., et al. (2017). Reduced biomass burning emissions reconcile conflicting estimates of the post-2006 atmospheric methane budget. *Nature Communications*, *8*(1), 2227. https://doi.org/10.1038/s41467-017-02246-0

Yin, Y., Chevallier, F., Ciais, P., Bousquet, P., Saunois, M., Zheng, B., et al. (2021). Accelerating methane growth rate from 2010 to 2017: Leading contributions from the tropics and East Asia. *Atmospheric Chemistry and Physics*, *21*(16), 12631–12647. https://doi.org/10.5194/acp-21-12631-2021

Zhang, L., Tian, H., Shi, H., Pan, S., Chang, J., Dangal, S. R., et al. (2022). A 130-year global inventory of methane emissions from livestock: Trends, patterns, and drivers. *Global Change Biology*, *28*(17), 5142–5158. https://doi.org/10.1111/gcb.16280

Zhang, Z., Poulter, B., Feldman, A. F., Ying, Q., Ciais, P., Peng, S., & Li, X. (2023). Recent intensification of wetland methane feedback. *Nature Climate Change*, *13*(5), 430–433. https://doi.org/10.1038/s41558-023-01629-0

Zhang, Z., Poulter, B., Knox, S., Stavert, A., McNicol, G., Fluet- Chouinard, E., et al. (2021). Anthropogenic emission is the main contributor to the rise of atmospheric methane during 1993–2017. *National Science Review*, *9*(5), nwab200. https://doi.org/10.1093/nsr/nwab200

Zhao, Y., Saunois, M., Bousquet, P., Lin, X., Berchet, A., Hegglin, M. I., et al. (2020). On the role of trend and variability in the hydroxyl radical (OH) in the global methane budget. *Atmospheric Chemistry and Physics*, *20*(21), 13011–13022. https://doi.org/10.5194/acp-20-13011-2020